minerals

MDPI

Article

Petrogenesis of the Granitic Dykes in the Yangshan Gold Belt: Insights from Zircon U-Pb Chronology, Petrography, and In-Situ Hf Isotope Analysis

Zhonghu Yang [1,2], Jianzhong Li [1,2,*], Tao Xiong [2], Yong Huang [2], Ciren Lamu [2], Yang Zhao [2] and Wei Wei [2]

[1] College of Earth Science, Chengdu University of Technology, Chengdu 610059, China; yangzhonghu@stu.cdut.edu.cn
[2] Research Center of Applied Geology, China Geological Survey, Chengdu 610036, China
* Correspondence: KCTZZX@126.com

Abstract: The Yangshan gold belt is renowned for its igneous rock formations, particularly dykes that form in tectonically weak zones. Some of these rock formations exhibit a close spatial relationship with gold mineralization, and a tiny portion of the granitic dykes serve as gold ore bodies by themselves. In order to investigate the nature of granitic dykes and their association with gold mineralization, we conducted a comprehensive study consisting of zircon U-Pb chronology, petrography, and in situ Hf isotope analysis of 25 granitic dyke samples collected from east to west across the belt. According to LA-ICP-MS zircon U-Pb dating results, the granitic dykes inherited zircon ages that are concentrated between 745.0 and 802.0 Ma, and magmatic intrusion ages that mainly fall between 201.0 and 213 Ma. Moreover, the granitic dykes display a calc-alkaline to high-K calc-alkaline peraluminous series, which is relatively enriched in light over heavy REE, with moderate Eu anomalies. These dykes are rich in large-ion lithophile elements and poor in high-field-strength elements. The zircon Lu-Hf isotope data range from εHf(t) values of -1.5 to 0.1, mantle model ($T_{DM}{}^1$) ages range from 859 to 937 Ma, and crustal model ($T_{DM}{}^2$) ages range from 1111 to 1218 Ma. The granitic dykes found in the Yangshan gold belt were formed between 200 and 213 Ma ago, during a period of intracontinental extension following the late collision between the Yangtze plate and Qinling microplates. These dykes originated from the volcanic basement of the Mesoproterozoic Bikou Group, which was formed by the melting of the upper crust under the crustal thickening caused by the subduction and collision of the Qinling microplate. Subsequently, the dykes were transported along a tectonically weak zone, assimilating surrounding rocks and undergoing a transformation from "I"-type to "S"-type granite before finally evolving into granite with specific "A"-type characteristics. Our study provides new insights into the petrogenesis of granitic dykes in the Yangshan gold belt, as well as the relationship between gold mineralization and magmatic activity, which has significant implications for mineral exploration and the geological understanding of gold mineralization in this region.

Keywords: Western Qinling Orogen; Yangshan gold belt; granite dykes; geochemistry; zircon chronology; Hf isotope

check for updates

Citation: Yang, Z.; Li, J.; Xiong, T.; Huang, Y.; Lamu, C.; Zhao, Y.; Wei, W. Petrogenesis of the Granitic Dykes in the Yangshan Gold Belt: Insights from Zircon U-Pb Chronology, Petrography, and In-Situ Hf Isotope Analysis. *Minerals* **2023**, *13*, 718. https://doi.org/10.3390/min13060718

Academic Editor: Hossein Azizi

Received: 16 April 2023
Revised: 18 May 2023
Accepted: 21 May 2023
Published: 24 May 2023

1. Introduction

The Yangshan gold belt is located in the Mian-Lue suture zone of the Western Qinling Orogen, which is situated between the western side of the Songpan-Ganzi terrane, the northern edge of the Yangtze Plate, and the southern edge of the Qinling microplates within the Wenxian arc-shaped tectonic system [1,2]. The Wenxian arc tectonic belt hosts several medium-to-large and super-large gold deposits, including Lian-hecun, Xinguan, Yangshan, Tangba, and Huachanggou, which are distributed along weak tectonic zones. Although there has been significant magmatic activity in both the Eastern Qinling Orogen and the Northern subbelt of the Western Qinling Orogen, Late Indosinian igneous rocks are almost absent in the western part of the Mian-Lue suture zone, except for a small amount in the

Bikou terrane on the northern margin of the Yangtze plate. Instead, they are mostly present in vein-like or lens-like shapes or rock walls along regionally weak tectonic zones. Based on extensive exploration works comprising over 200,000 m of core drilling, more than 15,000 square meters of pits, 427,500 square meters of trenches, and surface verification, the granitic dykes in this area mainly consist of granodiorite, fine-grained granite, biotite granite, and granite-porphyry dykes, with only a few fine-grained dykes visible.

An analysis of drilling results from the Yangshan gold deposit indicates that approximately 15% of granitic dykes contain gold mineralization and some local rock bodies are gold ore bodies. Previous research on magmatic evolution and metallogenesis show a temporal-spatial coupling relationship between granitic dykes and gold mineralization.

Both surface and drill hole granitic dykes exhibit obvious alteration characteristics, with the degree of alteration being negatively correlated with the integrity of the dykes. The main types of observed alterations include silicification, sericitization, chloritization, kaolinization, and epidotization, with less carbonate alteration. Quartz veins and fine quartz veins are also commonly observed in granitic dyke cores, with some occurrences displaced due to thrusting or extensional deformation, indicating ongoing tectonic activity. While most granitic dykes develop joints (generally 15–20 m), some earlier formed dykes exhibit weak cleavage deformation, suggesting their crystallization period may still be at a late stage when regional metamorphism dominated cleavage formation. Based on previous zircon U-Pb dating results of magmatic rocks [3–11], dykes with weak cleavage have a crystallization age mainly distributed around 215–220 Ma, while the crystallization age of non-cleavage granite porphyry dykes is concentrated around 212 Ma. The crystallization age of fine-grained granite dykes and fine-grained rock dykes is concentrated between 210–200 Ma.

This paper establishes a correlation between the crystallization age of medium-fine granite porphyry dykes and the metallogenetic age of the Yangshan gold deposit by analyzing previous geochronological data. Studying these granite dykes can provide insight into the regional characteristics of gold mineralization and geological background. Therefore, this paper aims to systematically investigate the types, petrographic, geochronological, and geochemical characteristics of granite dykes in the area, and to constrain tectonic activity during the magmatic activity period. The results will shed light on the subduction-collision process for the Wenxian arc-shaped tectonic belt in the western part of the Mian-Lue suture zone and promote a better understanding of the genesis type for gold deposits within the Yangshan gold belt.

2. Regional Geology and Geology of Deposits

2.1. Regional Geology

The Yangshan gold belt is situated between the Yangtze Plate, the North China Plate, and the Songpan-Ganzi orogenic belt, creating an "inverted triangle" geotectonic position. The geographical coordinates are: East longitude: 104°29′30″–105°00′00″; North latitude: 33°00′30″–33°10′00″ (see Figure 1) [1,2,12–16]. The regional stratigraphy ranges from Mesoproterozoic to Quaternary, including the Mesoproterozoic Bikou Group, found in the southeastern part of the area in the Motianling thrust tectonic zone. This group is primarily composed of shallow metamorphic volcanic-sedimentary rocks consisting mainly of tuffs, dolomites, and sandstones. Devonian strata are widely exposed and consist of a series of giant thick shallow marine clastic mudstone-carbonate sedimentary rocks. Carboniferous crops outs are around the Wenxian arc tectonic zone and comprise a series of coastal shelf-phase carbonate sedimentary formations, mainly thick layered limestone. Rocks of Permian are located in the northwest and southwest of the region and consist of marine carbonate rocks and normal sedimentary clastic rocks, primarily composed of tuffs, dolomitic tuffs, and sandstones. The Triassic period is also represented in the study area and includes coastal and shallow marine terrestrial clastic rocks with a small amount of carbonate rocks, primarily sandstone and sandy shale. The Jurassic series is found in the Puziba-Qiaotou-

Moba area and consists mainly of red sandy conglomerate sediment. In addition, there are large exposures of Cenozoic-Tertiary loess and Quaternary alluvial deposits [3,17,18].

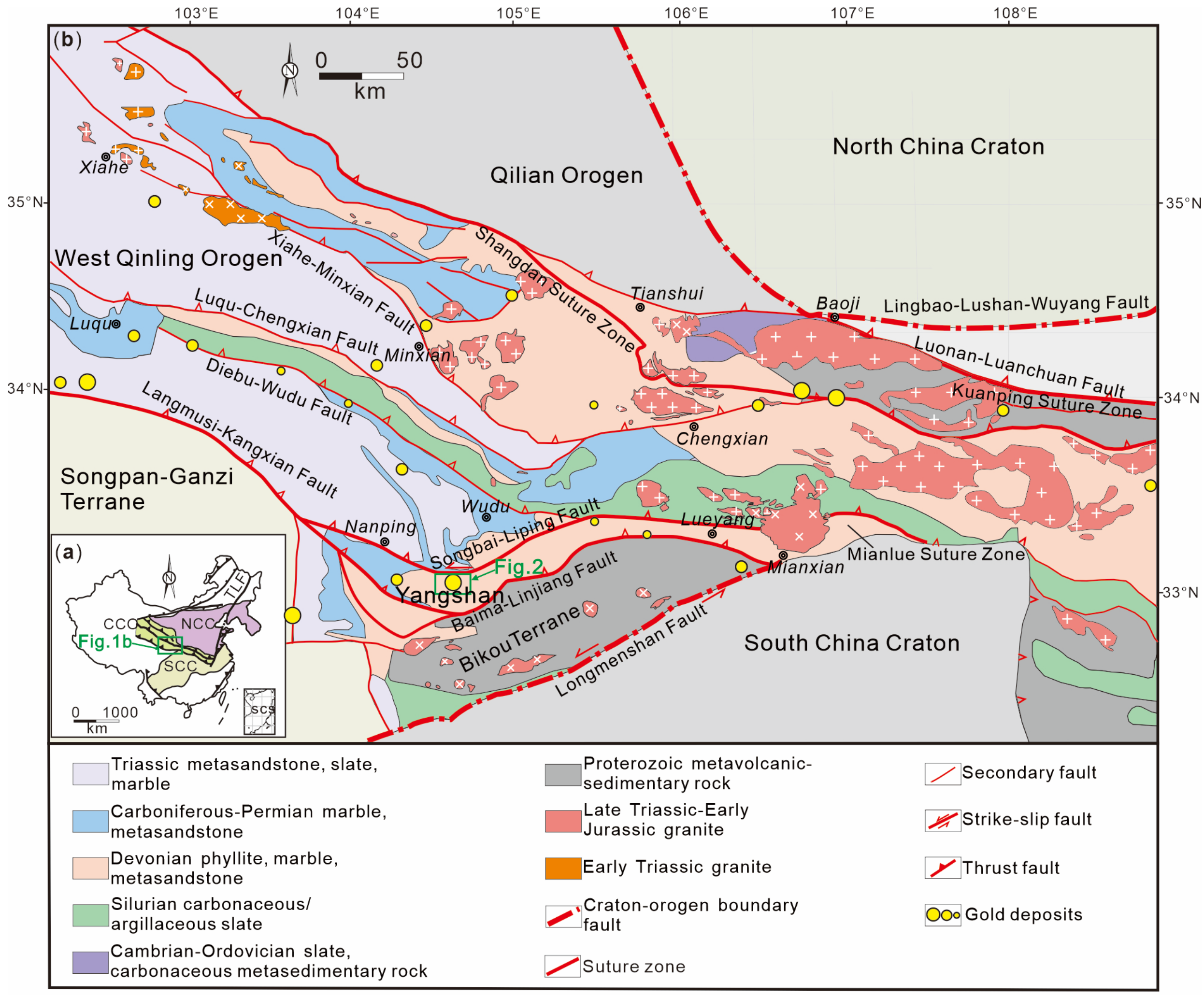

Figure 1. Simplified geological map of the West Qinling Orogen, showing the distribution of major crustal blocks, fault systems, and Mesozoic granitoids [16]. CCO, Central China Orogen; M, Mianlue; NCB, North China Block; SCB, South China Block; SCS, South China Sea; TLF, Tancheng–Lujiang Fault. (**a**): Tectonic overviews showing the position of West Qinling Orogen. (**b**): Schematic map showing the tectonic setting and distribution of gold deposits in West Qinling.

Magmatic rocks are widely distributed as dykes but typically do not form large-scale outcrops due to the superposition of multiple tectonic-magmatic events in the West Qinling orogenic belt. Previous studies have found that these rocks are widely exposed yet scattered, mainly along regional fractures or plate boundaries parallel to regional tectonic lines, and obviously controlled by regional tectonics. They form diverse types, with different lithologies of extrusive and intrusive rocks exposed, including tonalite porphyry, fine crystalline granite porphyry, and granite porphyry. Their formation is mainly related to three stages: the Caledonian-Variscan period, the Indosinian period, and the Yanshan period. Late Indosinian and Early Yanshan magmatic rocks are closely related to the time-space distribution of the Yangshan gold belt, although the relationship between magma and mineralization remains controversial [3,17,18].

The studied area comprises four arc-shaped retrograde thrust tectonic belts arranged in a zigzag pattern from north to south, with intricate backward and oblique folding structures mainly at the top of the arcs [1,2]. Figure 1 illustrates the four retrograde thrust tectonic zones within the West Qinling orogenic belt: Xiahe-Lixian, Luqu-Chengxian, Diebu-Wudu, and Langmusi-Nanping, also arranged from north to south. The folded structures are the Lixian-Xiahe dip-slope structure, the Luqu-Chengxian dip-slope structure, and the Bailongjiang (Diebu-Zhouqu) dip-slope structure, in order from north to south [1,2].

2.2. Geology of Deposits

The Yangshan gold belt is situated in the western part of the Mian-lue suture zone, which is a southern segment of the West Qinling Orogens. It is located at the top and to the east of the arc of the Wenxian tectonic zone [12–16]. The gold belt covers approximately 30 km, from Tang-bugou in the west to Guzhen in the east, and comprises six sections (see Figure 2). Among these, the Anba section has the highest confirmed gold reserves, constituting about 73% of the total reserves in the Yangshan gold belt [19].

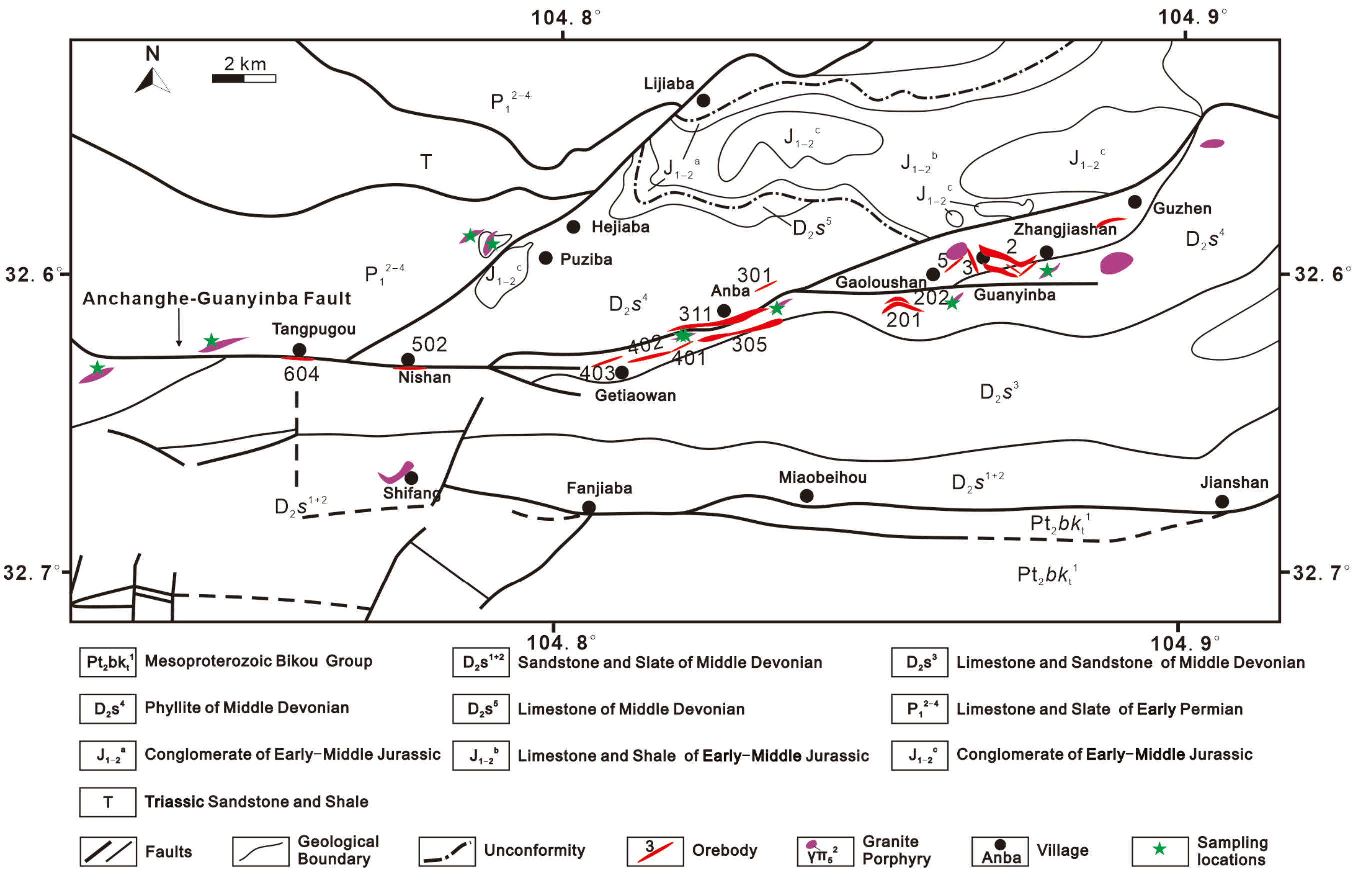

Figure 2. Simplified regional geology and deposit geology of the Yangshan gold belt (modified according to [7]).

The Yangshan gold belt is structured by the Caopingliang-Getiaowan complex back-slip and the Anchanghe-Guanyinba fault, with subsequent development of secondary faults, facies, lineaments, and associated structures. Ore bodies in the gold belt are mainly distributed on the two flanks of the Caopingliang complex dip, with the Anchanghe-Guanyinba fault and its secondary faults predominantly controlling their distribution [14,15]. The ore-bearing strata mainly consist of Devonian phyllites, fractured alteration rocks, some limestone, and a small number of dykes. Hydrothermal alteration includes silicification, sericitization, carbonatization, and the formation of kaolinite-montmorillonite, chlorite, and chlorite without any apparent zonation in space. Gold mineralization is most closely associated with silicification and sericitization [14,15].

The Yangshan gold belt hosts several medium felsic dykes, primarily composed of tonalite porphyry. Previously known as plagioclase granite porphyry, this paper adopts the IUGS igneous rock classification and refers to it as tonalite porphyry. Additionally, the belt contains fine-grained granite dykes, granite porphyry dykes, and tonalite porphyry dykes (see Figure 3). Table 1 summarizes the particular geological features of these dykes.

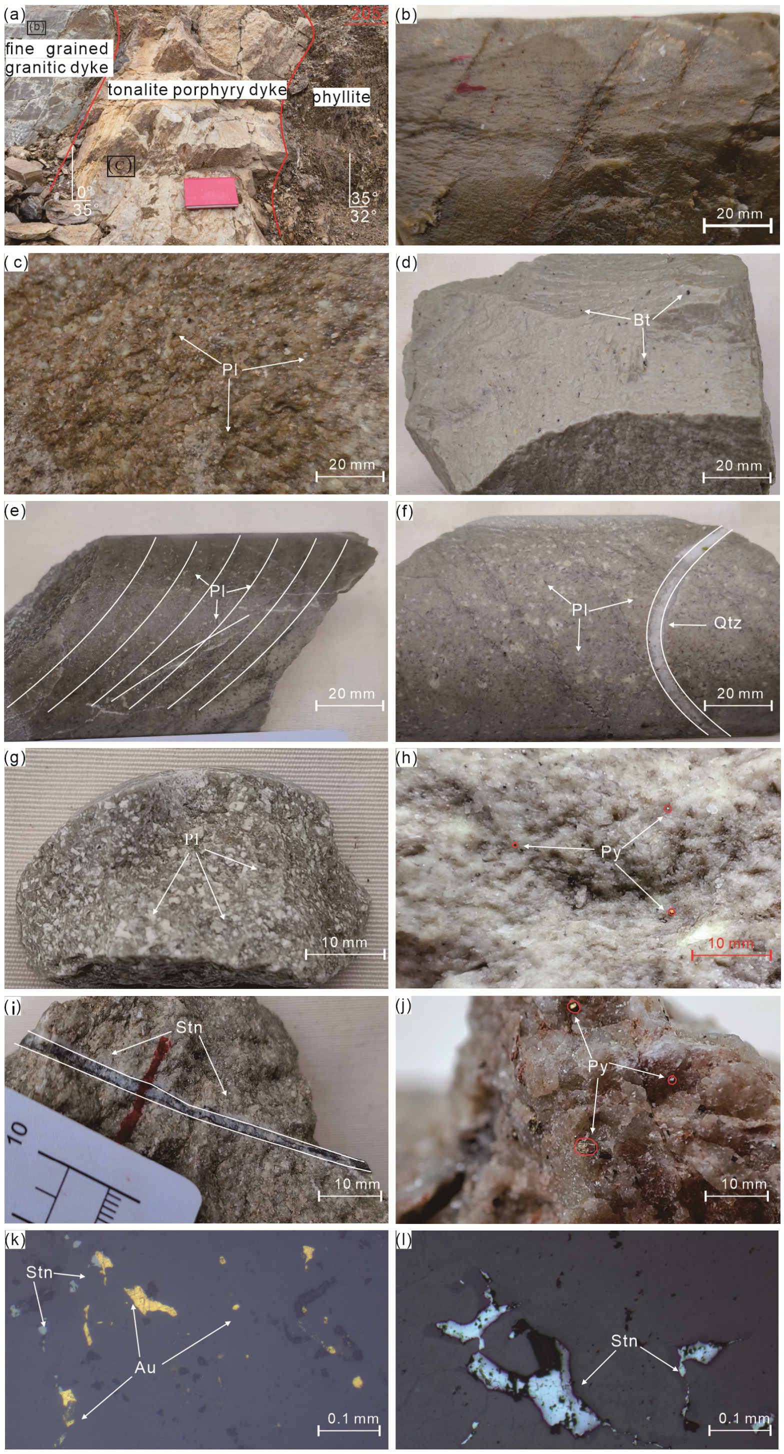

Figure 3. Granite dyke outcrops, dyke specimens, and mineralization photographs in the Yangshan gold belt. (**a**) a fine grained granitic dyke (**b**) intruded into a medium-coarse-grained tonalite porphyry dyke (**c**), field photo, Tangbugou, Nishan ore section; (**b**) a fine-grained granitoid dyke, with greenish joint development, no mineralization, Tangbugou, Nishan ore block; (**c**) a tonalite porphyry dyke with plagioclase phenocrysts, about 2–2 mm in size, the main components being plagioclase, quartz, a small number of dark minerals, no mineralization, Tangbugou, Nishan ore section; (**d**) a fine-grained

granitoid dyke, pale gray-green, with biotite grains, the sizes of which are about 2–2 mm, distributed in the fine-grained matrix, Sancai Mining Company, Getiaowan ore section; (**e**) a granite porphyry dyke, no obvious phenocryst, sericite, silicification and alteration developed, see sparse disseminated fine-grained pyrite, arsenopyrite, some particles are large, crack development, drill hole ZK4501, Gaoloushan ore section; (**f**) a granite porphyry dyke with a small amount of plagioclase phenocrysts, about 1.5–1.5 mm, sericitization and silicification developed, and stellated pyrite particles can be seen, with a size of 0.5–0.5 mm; (**g**) a tonalite porphyry dyke with a significant number of plagioclase phenocrysts, about 2–2 mm in size, showing signs of sericitization and silicification with stellated pyrite grains of about 0.5–0.5 mm in size, was found in drill-core ZK4501 of the Gaoloushan ore section; (**h**) a tonalite porphyry dyke with stellated pyrite mineralization, yellow-white and cube and pentagonal dodecahedron with idiomorphic and hypidiomorphic appearance, containing particles about 0.05 mm in size, was observed in drill hole ZK4501 of Gaoloushan ore zone; (**i**) a granite porphyry dyke with stibnite vein distribution along with fracture quartz veinlets, measuring 3 mm wide and 10 cm long, and with pyrite and arsenopyrite mineralization with star-like distribution was observed at No. 311 vein of Anba ore section at Mingjindong; (**j**) a highly silicified and sericitized granite porphyry dyke with pyrite grains with stellated distribution, measuring about 1.5–1.5 mm and being idiomorphic and hypidiomorphic, showing pentagonal octahedron appearance, was found at No. 311 vein of Anba ore body in Mingjindong; (**k**) a gold mineralized granite porphyry dyke in which the gold is mainly distributed in the quartz veinlets, measuring about 0.01 mm to 0.1 mm in size, showing golden luster and associated with stibnite was observed at No. 311 vein of Anba ore section in Mingjindong; (**l**) a granite porphyry dyke containing stibnite mineralization, having a smoky gray color, distributed in quartz dykes in a long strip about 0.1–0.3 mm in size, was found in No. 311 vein of Anba ore section in Mingjindong. Pl—plagioclase; Qtz—quartz; Bt—biotite; Stn—stibnite; Py—pyrite; Au—gold.

The dykes are primarily situated along a northwest-to-northeast direction within the deposit area, following the tectonic fault zone. These dykes range in width from half a meter to thirty meters and can span tens to hundreds of meters. The local wall rocks consist mainly of calcareous, carbonaceous, and calcareous phyllites from the Devonian Sanhekou Group. The contacts between the dykes and the wall rocks are predominantly intrusive, with some wall rocks displaying pyrometamorphism and contact metamorphism. The tonalite porphyry dykes, granite porphyry dykes, and fine-grained granitic dykes exhibit the strongest correlation with gold mineralization among the dyke types. These dykes host whole-rock gold mineralization with higher gold grades near the contact zone with the phyllite. In contrast, other dyke types such as quartz diorite dykes, biotite granite dykes, and granodiorite dykes display a weaker association with gold mineralization. Regarding age, the intermediate to felsic dykes exposed at the surface and in shallow caves within the Yangshan gold belt are primarily Late Triassic to Early Jurassic (209–171 Ma), with only a few instances of Early Cretaceous (116 Ma) and Eocene (51.2 Ma) zircon grain ages [3–12,17,18,20–22]. The age of the granite dykes falls within the onset of large-scale collisional granite formation in the West Qinling Orogeny (220–205 Ma). The detailed ages of granite dykes are shown in Table 2. The primary mineralization stage temperature is estimated to be between 300 and 210 °C [23], while the subsequent mineralization stage occurred between 288.3 and 271.3 °C [24]. The nature of the mineralizing hydrothermal fluid suggests that it was of medium to low temperature, implying that the mineralization took place slightly after regional metamorphism and magmatism.

Table 1. Geological characteristics of granitic dykes in the Yangshan gold belt [8].

Rock Name	Distribution Range	Scale	Brief Description	Petrographic Characteristics
Tonalite porphyry dykes	The most widespread, from Lianhe Village to Tangbugou to Zhangjiashan.	Usually a few meters to tens of meters wide, tens to hundreds of meters long.	The dykes are mostly intruded ininto Devonian and Triassic lithologies, often along or obliquely across the strata, and mostly in or near the fault zone. Multiple dykes often form a complex vein zone that has an intrusive contact relationship with the surrounding rock. The surrounding rock has often been experienced pyrometamorphism and contact metamorphism, the size of mineral particles in the dykes from coarse to fine., and local dykes have weak schistosity.	The tonalite porphyry is grayish white to light flesh red, the phenocryst composition is mainly plagioclase, their shape is elongated to platy, the grain size is generally 0.5–2 mm, about 45%; quartz, with grain size of 0. 5–1 mm, about 30%, and recrystallization; potassium feldspar, about 10%; dark minerals such as biotite and amphibole are mostly altered to sericite. The accessory minerals include magnetite, zircon, apatite, etc.
Quartz mica porphyry dykes	South of Gaojia Mountain, Guanyin Dam, Getiaowan and other places.	Small, with a width of one or two meters and a length of several meters to tens of meters.	The dykes intrude into Devonian strata controlled by fault zones and distributed in or near fault zones.	The rocks are porphyritic, and the phenocrysts are biotite and quartz, which make up 5–10% of the total. Matrix particles are relatively small. Under the microscope, it is mainly plagioclase, potassium feldspar and quartz.
Granite porphyry dykes	Lianhe Village, Shiji Dam and other places.	Small, about 10 m wide and several meters to hundreds of meters long.	The dykes are mainly in Carboniferous and Triassic strata, and locally the Devonian strata of the Sanhekou Group can be seen.	The fresh surface of the rock is grayish white, and the weathered surface is yellow-red brown, with granitic porphyritic structure. Feldspar phenocrysts, about 5%, with a grain size of 0.15–0.5 mm, and a few up to 2 mm, mainly plagioclase; quartz phenocrysts, about 4%, the dissolution is rounded, with wavy extinction, a small amount of muscovite phenocrysts; the matrix is felsic, mainly quartz, and less feldspar.
Fine-grained granite dykes	Guojiapo, Tangbugou, Getiaowan and other places.	The width is less than two meters and the length is less than two hundred meters.	It is often associated with the tonalite porphyry dykes, intruding or cutting through the tonalite porphyry dykes, and forming a contact metamorphism.	The rock is bright green, the mineral composition is mainly plagioclase with elongated or platy shapes, the grain size is generally 0.2–0.5 mm, about 35%; quartz, with grain size of 0.2–0.5 mm, about 35%, and recrystallization; the content of potassium feldspar is less, about 20%; dark minerals are mostly altered to sericite, and the false appearance of these dark minerals can be seen locally. The accessory minerals include magnetite, zircon, apatite, etc.

The Yangshan gold belt's dykes were formed during the Late Indosinian to Early Yanshan orogenic events, which represent the only period of mineralization in this belt. Thus, it is essential to conduct a comprehensive study of both mineralized and unmineralized granitic dykes encountered in drill holes and exposed at the surface. The goal of this study is to clarify the dykes' geological background, origin, evolution, and geochemical characteristics. These results will assist in the ongoing exploration of mineralization in the region.

Table 2. Previous results of dating granite dykes in the Yangshan gold belt.

Period	Testing Method and Age	Rock Type	Probable Geological Significance	References
Late Indosinian period	Zircon U-Pb age (224.5~207 Ma)	Tonalite porphyry, fine-grained granite, quartz porphyry dykes	The crystallization age	[8]
	Monazite U-Th-Pb age (220 ± 3 Ma)	Tonalite porphyry dykes	The upper limit of crystallization age	[17]
	K-Ar age (196~174 Ma)	Intermediate-acid dykes	The crystallization age	[3]
	K-Ar age (209~171 Ma)	Tonalite porphyry dykes	The crystallization age	[4]
	Rb-Sr Isochron age (199.28 ± 42.79 Ma)	Granite porphyry dykes	The crystallization age	[20]
	Zircon LA-ICP-MS U-Pb age (217~211 Ma)	Granite dykes	The crystallization age	[9]
	Muscovite ^{40}Ar-^{39} Ar Plateau age (220.4~211.1 Ma)	Granite porphyry dykes	The crystallization age	[10]
	Zircon LA-ICP-MS U-Pb age (202~190 Ma)	Granite porphyry dykes	The crystallization age	
	Zircon LA-ICP-MS U-Pb age (215.3~210.8 Ma)	Granite porphyry dykes	The crystallization age	[21]
	Zircon LA-ICP-MS U-Pb age (216.5~214.8 Ma)	Tonalite porphyry dykes	The crystallization age	[22]
Yanshan period	Zircon U-Pb age (114.6~118.1 Ma)	Fine-grained tonalite dykes	The crystallization age	[15]
	Zircon in quartz veinlets U-Pb age (195.4~200.9 Ma)	Captureing zircons from late Triassic and early Jurassic tonalite porphyry dykes	The crystallization age	[5]
	Zircon in quartz veinlets U-Pb age (126.9 ± 3.2 Ma)	Capturing zircons from Cretaceous concealed magmatic rock	The crystallization age	[5]
	Zircon LA-ICP-MS U-Pb age (177.7 ± 2.9 Ma)	Tonalite porphyry dykes	The crystallization age	[22]
Himalayan period	Zircon in quartz veinlets U-Pb age (51.2 ± 1.3 Ma)	Capturing zircons from the Tertiary concealed magmatic rock	The crystallization age	[5]
	Zircon LA-ICP-MS U-Pb age (49.5 ± 1.8 Ma)	Fine-grained tonalite dykes	The crystallization age	[22]

3. Sampling and Methods

3.1. Sampling

The Yangshan gold belt presents challenges for sample collection due to a thick loess layer and poor bedrock exposure. To address this, surface exposures at various locations were sampled, as well as granitic dykes encountered by drilling and trenching. A total of 25 samples were collected for zircon single mineral separation, out of which 9 samples were chosen for further analysis. Zircon LA-ICP-MS dating was performed on the selected 9 samples, whereas whole rock trace element analysis was conducted on all 25 samples. However, some single-grain zircons were too small to be analyzed reliably for Lu and Hf isotopes, so only two samples underwent in situ Lu-Hf isotopic testing.

Nine samples were collected for further analysis. The majority of these samples are tonalite porphyry, granite fine-crystalline dykes, and granite porphyry dykes. Specific information on the samples is provided in Table 3, while their distribution locations are shown in Figure 2. Hand specimens and microscopic photographs of the samples are illustrated in Figures 3 and 4, respectively.

Table 3. Sampling localities and description of samples investigated in this study.

Ore Block	Sampling Location	Sample Number	Field Naming	Sample Description
Zhangjiashan	N: 33.080592° E: 104.782187° H = 1829.68 m	21ZJS01	Granite porphyry dykes	Pyrite mineralization and minor alteration
Guanyinba	N: 33°3′21″ E: 104°38′44″ H = 1273.8 m	TC2101	Granite porphyry dykes	Granite porphyry dykes, relatively fresh, no obvious alteration, gray-green, joint development of multiple groups
Anba	N: 33°3′14″ E: 104°38′44″ H = 1735.9 m	311-8-1	Granite porphyry dykes	Pyrite mineralization, arsenopyrite mineralization, quartz vein gold mineralization
Anba	N: 33°3′14″ E: 104°38′44″ H = 1735.9 m	311-8-6	Granite porphyry dykes	Pyrite mineralization, arsenopyrite mineralization, quartz vein gold mineralization
Anba		ZK1798-1	Granite porphyry dykes	Pyritization, almost unchanged
Getiaowan	N: 33°3′29″ E: 104°37′28″ H = 1126.6 m	21SCKY01	Fine-grained dykes	Coarse mica flake and pyrite mineralization were observed, but no obvious alteration was observed
Nishan	N: 33°3′35″ E: 104°37′8″ H = 1266.5 m	21PZB01	Granite porphyry dykes	Medium-coarse grained granite porphyry, large-grained pyrite
	N: 33°3′28″ E: 104°38′25″ H = 1673.3 m	21NS01	Granite porphyry dykes	Medium-coarse grained granite porphyry, plagioclase porphyry, no mineralogical alteration
Guojiapo	N: 33°1′27″ E: 104°29′35″ H = 1535.8 m	BS2101	Granite porphyry dykes	The medium-coarse grained granite dyke was intruded by fine-grained granite
Xiguan	N: 33°3′46″ E: 104°26′49″ H = 1273.8 m	XG2101	Granite porphyry dykes	The granite porphyry dykes were more broken and strongly altered, and no mineralization was observed

The Zhangjiashan section sampling site contains medium- to fine-grained granite porphyry dykes with weak alteration, well-developed bedding rock joints, and a relatively fragmented structure. The samples collected from this field are gray-white to gray in color, with mottled and block-like structures, and are classified as granite porphyry dykes. The porphyritic crystals have a size of about 1.0–1.5 mm and mainly consist of plagioclase (40%) and quartz (30%). The matrix is primarily composed of quartz and plagioclase (30%). The dykes exhibit kaolinization and chloritization, but no pyritization was observed.

At the Guanyinba sampling site, granite dykes intrude fragmented and altered phyllite. The rock is gray-white granite porphyry with a mottled and block-like structure. Porphyritic crystals are primarily plagioclase (40%) and quartz (30%), distributed in a mottled pattern with a size of 1.5–2.0 mm. The matrix comprises quartz (15%), plagioclase (10%), and chlorite (5%). Chloritization is the primary alteration type. The dykes' integrity is well preserved, showing its original shape. The contact surface with the underlying phyllite is arched at an average angle of about 40°. Gold mineralization is visible within and around the dykes, with Au grades of 14.9 g/t in the dyke and 8.29 g/t in the phyllite. The gold enrichment may be due to surface oxidation leaching of the primary ore, implying the possibility of magmatic-hydrothermal mineralization, but further evidence is required.

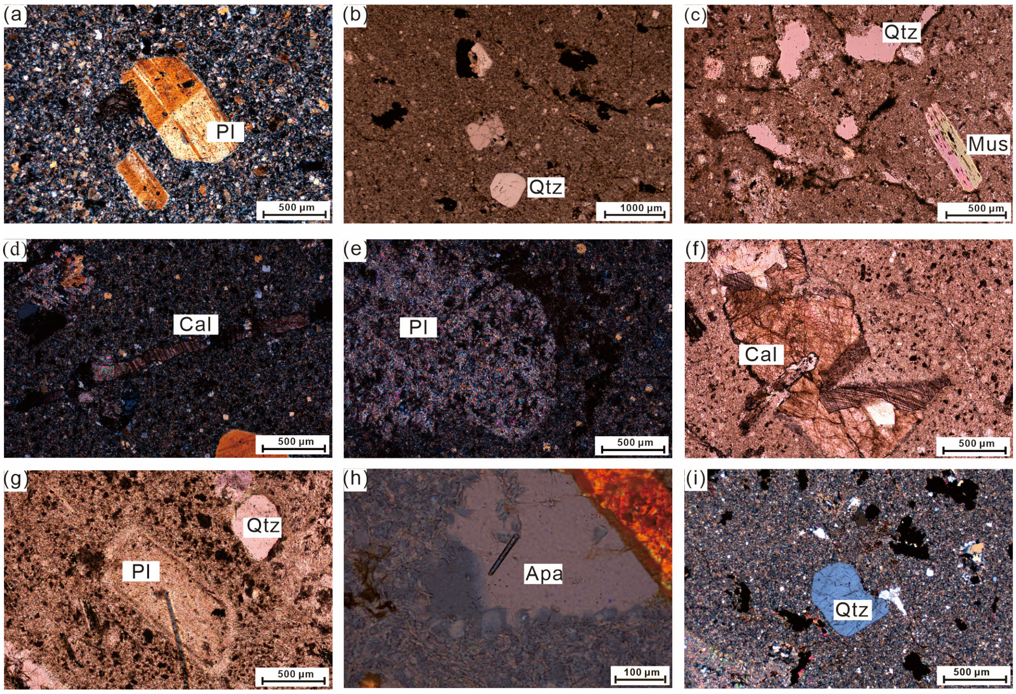

Figure 4. Petrographic microphotographs of granite dykes. Samples include: (**a**) 21SCKY03, a fine-grained dyke composed of granite with small quantities of plagioclase phenocrystal, quartz, and carbonate, showing visible arsenopyrite mineralization under crossed polarizers; (**b**) TC2101-04, a granite porphyry containing quartz porphyry and biotite, visible under parallel polarizers; (**c**) feldspar, quartz, biotite porphyry in ZK6901 granite-porphyry, visible under crossed polarizers; (**d**) calcite vein in granite-porphyry ZK6903-01, visible under crossed polarizers; (**e**) feldspar porphyry in granite-porphyry ZK6903-01 replaced by argillite, visible under crossed polarizers; (**f**) feldspar and carbonate porphyry in granite-porphyry ZK6903-01, visible under parallel polarizers; (**g**) feldspar porphyry in granite porphyry ZK6903-02 replaced by clay minerals, visible under parallel polarizers; (**h**) apatite in granite porphyry TC2101-04, visible under crossed polarizers; (**i**) quartz porphyry in granite porphyry TC2101-04, visible under crossed polarizers. The abbreviations used for minerals are Pl—feldspar, Qtz—quartz, Mus—muscovite, Cal—calcite, Bt—biotite, Apa—apatite.

At the Anba sampling site, gray-green granitic porphyry dykes with a medium-fine grain and mottled structure occur. The porphyritic crystals have a grain size of approximately 1.0–1.0 mm and consist mainly of quartz (35%) and plagioclase (35%). The matrix contains quartz (10%) and feldspar (10%). Pyrite and arsenopyrite are present in the dyke. Pyrite is fine-grained and stellated, idiomorphic and hypidiomorphic, while arsenopyrite is silver-white, acicular, measuring about 0.5–2~3 mm in length, and idiomorphic. Visible gold mineralization has been observed in nearby drill holes.

At the Getiaowan section sampling site, outside the mine tunnel of Sancai Mining Company, lies a gray-green fine-grained dyke with a blocky texture and fine-grained structure. The main components of the dyke are quartz (65%), feldspar (30%), and dark mica (5%). Although the sample is well-preserved with no visible alteration, sporadic cubic particles of pyrite with a size of approximately 2.0–2.0 mm are dispersed throughout the dyke.

At the Nishan section sampling location, the two dykes exhibit remarkable similarities in their mottled structure and blocky texture. They predominantly display gray and gray-white colors. The porphyritic crystals mainly comprise plagioclase (35%) and quartz (30%), with an average grain size of approximately 1.5–2.0 mm. The dyke matrix primarily consists of quartz and plagioclase (30%), with a small fraction of thin, platelike dark minerals (5%) suspected to be biotite. Upon examination, the dykes appear to exhibit a high degree of structural integrity, devoid of apparent alteration or mineralization.

At the Guojiapo sampling location, fine-grained dykes of greyish green intrude into medium-fine-grained granite porphyry dykes. The former exhibits very-fine-grained and massive structures, consisting mainly of feldspar and quartz with evident dyke joints and no mineralization. In contrast, the gray to gray-brown medium-fine granitic porphyry dykes show a porphyry structure. The porphyritic crystals of plagioclase (40%) and quartz (35%) exhibit a porphyry grain size of approximately 1.5–2.0 mm, while the matrix consists mainly of quartz and plagioclase (20%) with minor dark minerals (5%). Although weakly altered, these dykes maintain a high degree of structural integrity and appear to intrude into the contact boundary of surrounding rocks, showing visible contact metamorphism phenomena in phyllite without apparent displacement of the contact boundary.

The Xin Guan sampling location exhibits granite dykes that intersect with carbonaceous phyllites and thin-bedded tuffs within the area. The dykes display significant deformation and kneading and have been truncated by late tectonic faulting activities. Granitic porphyry dykes at this site possess a gray-white to gray-brown coloration, medium to fine-grained texture, and massive structure. Porphyritic crystals are predominantly plagioclase (35%) and quartz (40%), with a grain size of about 1.5–2.0 mm. Furthermore, the matrix is primarily composed of plagioclase and quartz (30%), alongside some dark minerals (5%). The hand specimen is highly fragmented and altered, with kaolinization and chloritization being the dominant alteration processes. No discernible mineralization is evident.

3.2. Analytical Methods

In the laboratory of Guangzhou Tuoyan Testing Technology Co., Ltd. (Guangzhou, China), zircon single mineral selection, target preparation, and cathodoluminescence (CL) photography were conducted using a high-vacuum scanning electron microscope (JSM-IT100) equipped with the GATAN MINICL system. Zircon LA-ICP-MS dating was performed in the laboratory of Wuhan SampleSolution Analytical Technology Co., Ltd. (Wuhan, China) using an Agilent inductively coupled plasma mass spectrometer (Agilent 7900) and a coherent 193 nm excimer laser ablation system (GeoLas HD). Standard samples used for this analysis include NIST610 for trace element calibration, 91,500 for isotope ratio calibration, and GJ-1 for isotope ratio monitoring. ICPMS-DATACAL10.8 processing software was used, and laboratory cleanliness was maintained below the 1000 level. For quality control, the analysis sequence of the NIST610/2 91,500/2 GJ-1/6 samples (U-Pb age)/2 91,500/2 GJ-1/2 91500/NIST610) was employed. Details of the analytical conditions and procedures can be found in Liu et al. (2008, 2010) [25,26].

Whole-rock major and trace element analyses were carried out at the Guangzhou Tuoyan Testing Technology Co., Ltd. laboratory using an Agilent 720 ICP-MS. Detailed conditions and procedures for major and trace element analyses are given in Potts et al. (2005) [27].

In situ Hf isotope ratio analysis of zircon was performed using laser ablation multi-collector plasma mass spectrometry (LA-MC-ICP-MS) at Wuhan SampleSolution Analytical Technology Co., Ltd. The laser ablation system used was Geolas HD and the MC-ICP-MS used was Neptune Plus. Details of the analytical conditions and procedures can be found in Hu et al. (2012a, 2012b) [28,29].

The εHf was calculated using the ^{176}Lu decay constant of $1.865 \times 10\ y^{-11-1}$ [30] and present-day values for chondrites of $^{176}Hf/^{177}Hf = 0.282772$ and $^{176}Lu/^{177}Hf = 0.0332$ [31]. The single-stage Hf model age (t_{DM1}) was calculated using the depleted mantle with present-day $^{176}Hf/^{177}Hf = 0.28325$, $^{176}Lu/^{177}Hf = 0.0384$, and the two-stage Hf model age (t_{DM2}) was calculated using the upper crustal average $^{176}Lu/^{177}Hf = 0.015$ [32].

4. Results

4.1. Zircon U-Pb Dating

Nine samples underwent zircon LA-ICP-MS dating, and the results are reported in Tables 4 and A1. The majority of zircon grains exhibit oscillatory zonation, with some retaining ancient zircon cores in bright white and gray colors. Most zircon grains appear grayish-black. Zircon Th/U ratios indicate that 243 out of 245 grains have ratios greater than 0.4, which is typical of magmatic zircon grains [33]. The average size of zircon grains is around 100 μm with an aspect ratio of 2:1, except for sample ZK1798-01 where individual zircon grains range from 100 to 200 μm and have an aspect ratio between 2:1 and 4:1. Figure 5 shows the ages of typical zircon grains plotted against their age values.

Table 4. Zircon LA-ICPMS U-Pb age of the Yangshan gold belt.

Sample No.	Lithology	Age (Ma)	Geological Significance
21BS-001	Medium-coarse grained granite dyke	786.74 ± 3.68 Ma (n = 18/18) MSWD = 27.0, p(x2) = 0	Inherited zircon age
21NS01	Medium-coarse grained plagioclase granite porphyry dyke	771.71 ± 3.68 Ma (n = 14/14) MSWD = 18.7, p(x2) = 0	Inherited zircon age
21PZB01	Medium-coarse grained plagioclase granite porphyry dyke	213.1 ± 1.6 Ma (n = 15/15) MSWD = 0.2, p(x2) = 1.0	Crystallization age of granite dykes
21XG01	Medium-coarse grained granite dyke	801.97 ± 4.73 Ma (n = 10/11) MSWD = 6.32, p(x2) = 0.0000000053	Inherited zircon age
21ZJS01	Medium-coarse grained granite vein	210.49 ± 1.50 Ma (n = 8/8) MSWD = 1.34, p(x2) = 0.23	Crystallization age of granite dykes
311-8-1	Granite porphyry dykes	213.3 ± 7 Ma (n = 2/2)	Crystallization age of granite dykes
311-8-6	Granite porphyry dykes	749.89 ± 4.86 Ma (n = 11/11) MSWD = 49.6, p(x2) = 0	Inherited zircon age
TC2101-02	Granite porphyry dykes	206.7 ± 2.8 Ma (n = 3/3) MSWD = 14, p(x2) = 0.000001	Crystallization age of granite dykes
ZK1798-1	Fine-grained granitic dykes	201.02 ± 0.83 Ma (n = 25/25) MSWD = 24.9, p(x2) = 0	Crystallization age of granite dykes

Sample 21BS-001, from which 18 points were selected, yields concordant ages with a mean $^{206}Pb/^{238}U$ of 786.74 ± 3.68 Ma (2σ, mean square of weighted deviations [MSWD] = 27). Yields from the second set of points are concentrated in the Paleoproterozoic and Mesoproterozoic, indicating the time of initial zircon formation. The origin of the zircon grains is believed to be from either the Devonian wall rocks or the deep basement of the Bikou Group and the volcanic clastic rocks of the Bikou Group in the Neogene.

Sample 21NS01, from which 14 points were selected, yields concordant ages with a mean $^{206}Pb/^{238}U$ of 771.71 ± 3.68 Ma (2σ, mean square of weighted deviations [MSWD] = 18.7). The second group of ages falls mainly into the Paleozoic and Middle Proterozoic. This finding suggests that these zircon grains originally formed during those periods. It is possible that these zircon grains originated from either the Devonian peridotite or the deep basement of the Bikou Group and the Neoproterozoic volcanic clastic rocks of the Bikou Group.

Sample 21PZB01, from which 15 points were selected, yields concordant ages with a mean $^{206}Pb/^{238}U$ of 213.1 ± 1.6 Ma (2σ, mean square of weighted deviations [MSWD] = 0.2). This age is considered to represent the crystallization age of the dyke. Other ages are concentrated in the Paleozoic and Middle Proterozoic, indicating the inherited zircons from other magmatic rocks.

Sample 21XG01, from which 11 measurement points were selected, yields concordant ages with a mean $^{206}Pb/^{238}U$ of 801.97 ± 4.73 Ma (2σ, mean square of weighted deviations [MSWD] = 6.32). Other ages are concentrated in the Paleozoic and Mesoproterozoic, indicating the inherited zircons from other magmatic rocks. The zircon grains in this sample possibly originated from the Devonian wall rocks, the deep basement of the Bikou Group, or the Neoproterozoic volcanic clastic rocks of the Bikou Group. Eight points from sample 21ZJS01 give concordant ages, with a concordant mean $^{206}Pb/^{238}U$ of 210.49 ± 1.5 Ma (2σ, mean square of weighted deviations [MSWD] = 1.34). This age is considered to represent the crystallization age of the dyke. Other ages measured were concentrated in the Paleozoic and Mesozoic, whereas a few others yield Triassic ages. These additional measurements represent the ages of zircon formation in metasedimentary and inherited igneous rocks from the wall rocks or the basement of the Bikou Group.

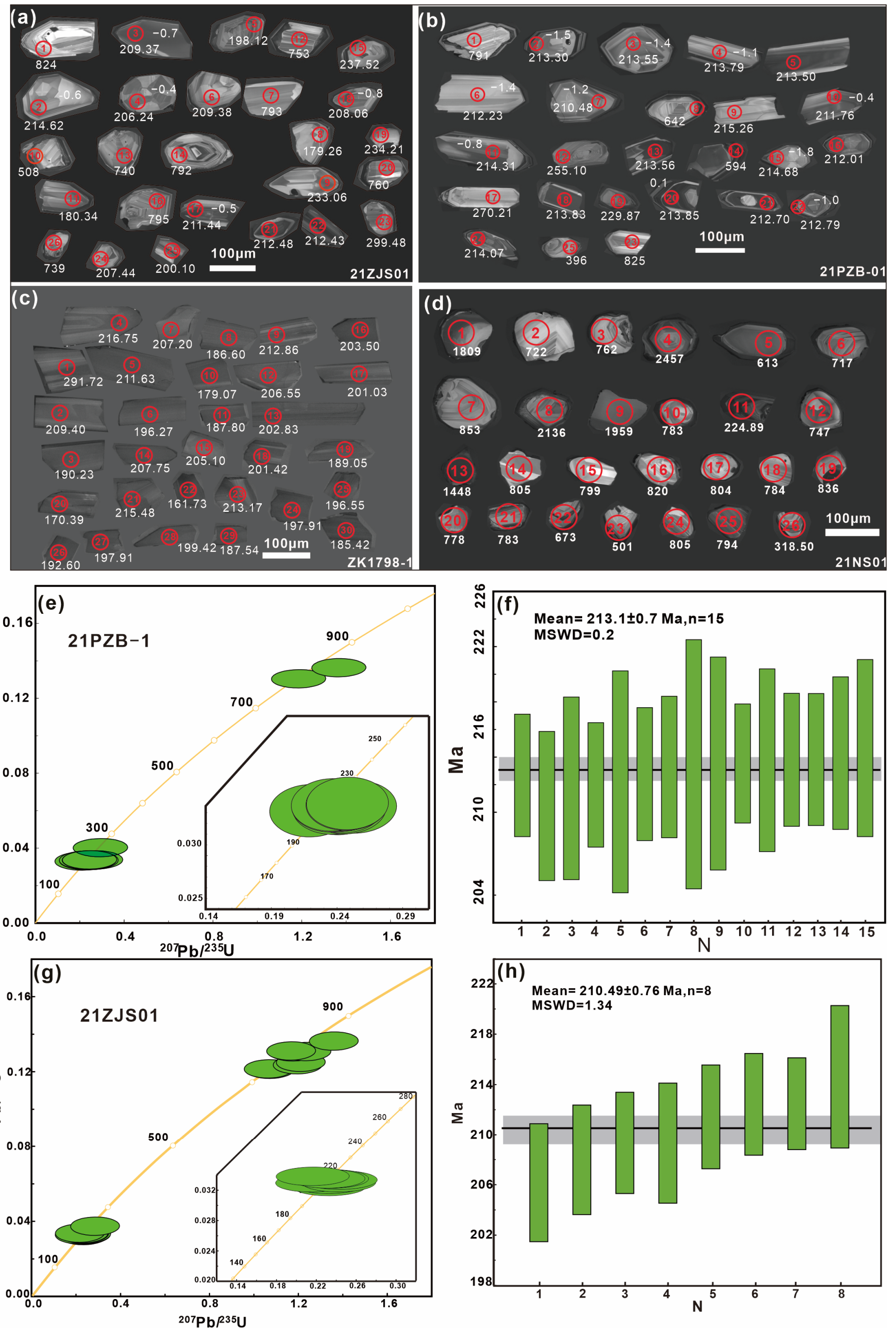

Figure 5. Zircon crystal morphology, U-Pb ages, εHf (t) values (**a**–**d**); concordia diagrams (**e**–**h**).

Sample 311-8-1 yielded 22 zircon grains, which mainly showed Mesoproterozoic, Neogene, Paleozoic, and Mesozoic ages. The Mesozoic ages, ranging from 211 to 215 Ma, represent the crystallization age of the granitic porphyry dykes. The remaining ages reflect zircon formation in the inherited magmatic rocks from the wall rocks or the basement of the Bikou Group. Sample 311-8-6 yielded 27 zircon grains, and the weighted average of 11 measurement points gives an age of 749.89 ± 2.48 Ma (n = 11/11), with an MSWD value of 49.6. Other ages are mainly Paleoproterozoic, Paleozoic, and Mesozoic, representing the age of inherited zircon formation from the wall rocks or the basement of the Bikou Group.

Among 30 zircon grains were examined from TC2101-02, most of the ages are the Mesoproterozoic, Neogene, Paleozoic, and Mesozoic. The crystallization age of the granitic porphyry dyke was determined by taking the weighted average of the three youngest data points, resulting in an age of 206.7 ± 1.2 Ma (n = 3/3). The remaining ages reflect zircon formation in metasedimentary and inherited igneous rocks from the peritectic rocks or the basement of the Bikou Group.

A total of 30 zircon grains from ZK1789-1 were selected for analysis. The weighted average of 25 measurement points yielded an age of 201.02 ± 0.42 Ma (n = 25/25), with an MSWD value of 24.9. This age represents the crystallization age of the granitic fine-crystal dyke. The remaining ages fall mainly into the Neogene and Mesozoic Triassic, and reflect zircon formation in metasedimentary and inherited magmatic rocks from the wall rocks or the Bikou Group basement.

4.2. Element Geochemistry

Nine granitic dyke outcrops were selected from west to east along the Anchanghe-Guanyinba ore control fracture zone in the Yangshan gold belt, and 25 samples were collected for major and trace element analysis. The data are reported in Table A2. The 25 samples were divided into ten groups by sampling location for data presentation and evaluation. Samples 21BS-02 and 21BS-03 are intrusive contact relations that are treated separately.

SiO_2 contents range from 71.99% to 84.53% with an average of 76.29%. Other ranges are: Al_2O_3 10.09%–17.29%, K_2O 2.12%–3.89%, Na_2O 0.08%–4.59%, TiO_2 0.02%–0.38%, CaO 0.43%–2.66%, and total iron as Fe_2O_3 0.43%–2.46%. The Rittman index (σ) varies between 0.30 and 1.87, indicating a calc-alkaline nature.

Based on lithological classification and SiO_2-Na_2O + K_2O relations, almost all samples fall into the granite field (Figure 6a), some on the boundary between granodiorite and granite. A/CNK and A/NK values range from 1.47 to 3.84 and 1.68 to 5.39, respectively (Figure 6c). All samples are peraluminous with values above 1.1. These data suggest that the granitic dykes studied are 'S-type' igneous rocks with calc-alkaline to high-K calc-alkaline characteristics (Figure 6b).

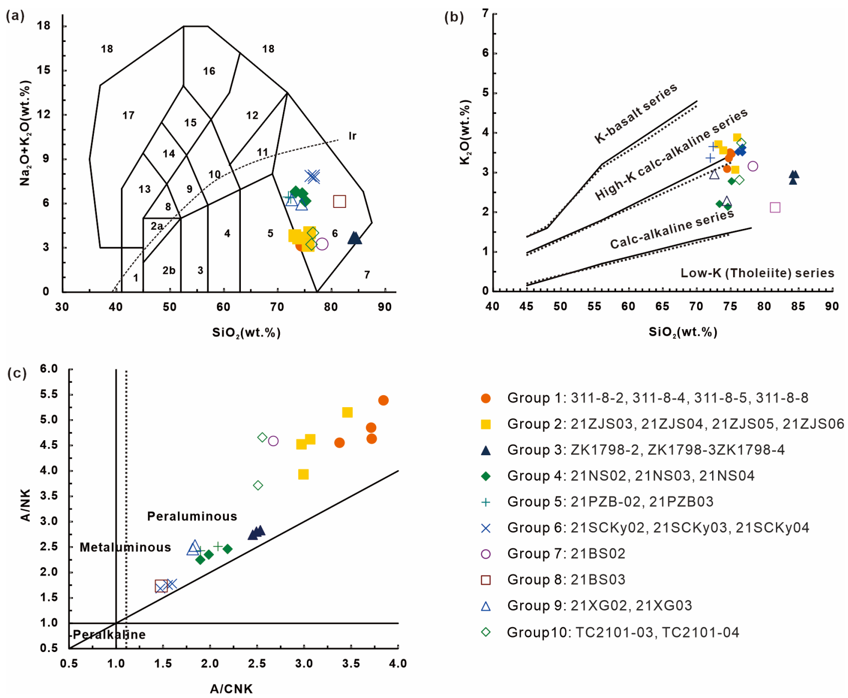

Figure 6. (Na_2O + K_2O) vs. SiO_2 (**a**), after Middlemost, 1994) [34]; K_2O vs. SiO_2 (**b**), after Rollinson, 1993) [35]; A/CNK vs. A/NK (**c**), [36]). (**a**), Ir: Irvine boundary, with alkaline above and subalkaline below. 1—olivine gabbro; 2a—syenogabbro; 2b—gabbro; 3—gabbro–diorite; 4—diorite; 5—granodiorite; 6—granite; 8—alkali–gabbro; 9—alkali–gabbroicdiorite; 10—syenodiorite; 11—quartz monzonite; 12—syenite; 13—feldspathoid gabbro; 14—feldspathoid monzonite diorite; 15—feldspathoid monzonitic syenite; 16—feldspathoid syenite; 17—foidite pluton; 18—leucite rock.

The total concentration of rare earth elements (ΣREEs) encompasses a wide range, from 16.17 to 96.69 ppm with a mean of 67.88 ppm. All samples show the enrichment of light REEs over heavy REEs. $(La/Yb)_N$ values range from 1.92 to 30.93. The chondrite-normalized REE patterns for a member of each group are shown in Figure 7a. The δEu (where $\delta Eu = Eu/(\sqrt{Sm} \times Gd)$, chondrite-normalized values) range from 0.45 to 0.85, with the four granitic dykes (21BS02, 21BS03, 21SCKy02, and TC2101-03) exhibiting the most significant Eu anomalies. The overall REE distribution curves are similar to those of granitic rocks. The δCe (where $\delta Ce = Ce/(\sqrt{La} \times Pr)$, chondrite-normalized values) range from 0.78 to 0.91 with a slight negative anomaly and an average value of 0.84. Two types of chondrite-normalized REE patterns can be identified in Figure 7a: (I) rocks with LREE enrichment, a small negative Eu anomaly, and low levels of HREEs, and (II) rocks with an inverted U-shaped pattern accompanied by a well-developed negative Eu anomaly. Additionally, rare earth elements in these samples are depleted relative to the continental crust, but the distribution pattern of light rare earth elements in some samples is similar to that of the upper and lower crust.

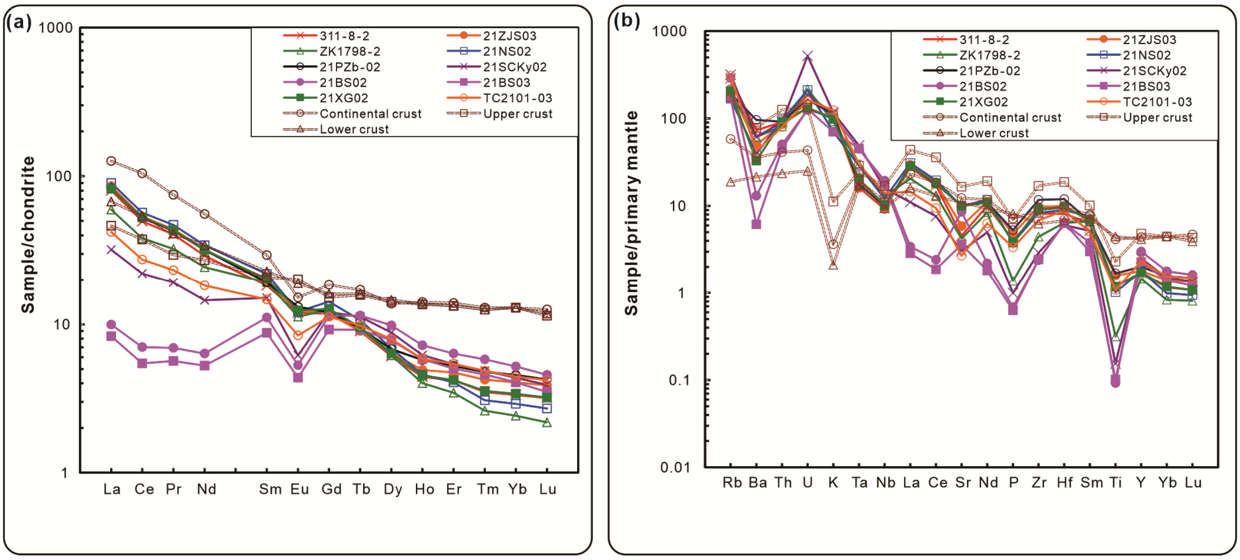

Figure 7. (**a**) Chondrite-normalized rare earth element (REE) patterns, (**b**) Primitive mantle–normalized spider diagram (chondrite(C1); primary mantle data is taken from Sun et al. (1989) [37], continental crust, upper crust, lower crust data is taken from Taylor et al. (1985) [38]).

Primitive-mantle-normalized trace elements for a member of each of the ten groups are displayed in Figure 7b. They exhibit significant positive anomalies for Rb, Th, and U, indicating an enrichment of large-ion lithophile elements, and exhibit significant negative anomalies for Ti and P, indicating loss of high-field-strength elements. Additionally, trace elements in these samples are mostly depleted relative to the crust except for some elements (Rb, Ba, Th, U, K, Ta, and Nb).

4.3. Zircon Hf Isotope

Lu-Hf isotope analysis was conducted on 16 zircon samples (sites) from the 21PZB-01 and 21ZJS-01 specimens, and the data are presented in Table A3. All zircon sites have $^{176}Lu/^{177}Hf$ ratios within the range of 0.000286 to 0.001655, which preclude the significant accumulation of radiogenic Hf after their formation. Thus, the measured $^{176}Hf/^{177}Hf$ ratios signify the Hf isotopic composition at the time of zircon formation. εHf(t) values range from −1.5 to 0.1(t), and most of the test points are located near the evolution line of chondrites (Figure 8). The age range for the mantle model ($T_{DM}{}^1$) can be estimated to be 859–937 Ma, whereas the range of crustal model ages ($T_{DM}{}^2$) is 1111–1218 Ma.

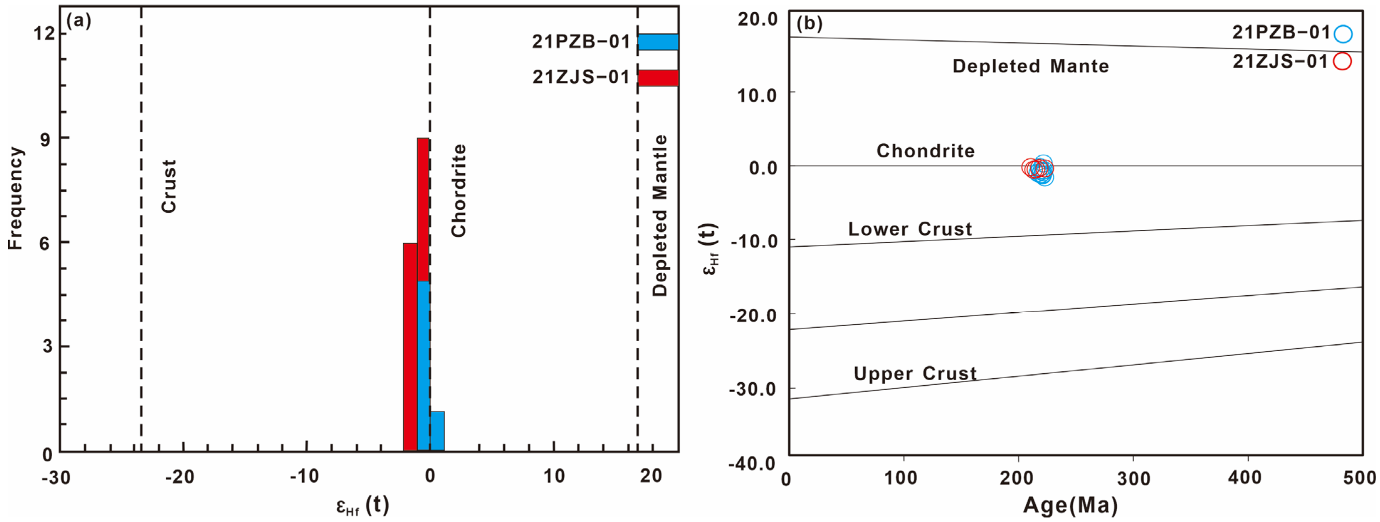

Figure 8. (**a**) a frequency diagram of εHf (t); (**b**), the Zircon U-Pb ages versus εHf (t) values.

5. Discussion

5.1. Petrogenesis

For this study, we have collected 25 samples from nine granitic dykes in the Yangshan gold belt. The samples were found to be high-potassium calc-alkaline granites, belonging to the peraluminous granite group with A/CNK values ranging from 1.47–3.84. These values indicate that they may be S-type igneous rocks, as all values are greater than 1.1. The Rb/Sr ratio has a mean value of 1.45 with a distribution range of 0.49–3.49, significantly higher than the global upper crustal mean of 0.32 [38]. Similarly, the Nd/Ta ratio had a mean value of 12.93 with a range of 1.32–22.98, partially higher than the global upper crustal mean of 12.0 [38]. Figure 7b shows positive anomalies of Rb, Ba, Th, U, K, and Ta, indicating the enrichment of crustal elements and suggesting that parts of the granitic dyke magmas are derived from upper crustal melting. The results are consistent with previous studies which suggest a close relationship between the granitic dykes and the stratigraphy of the Bikou Group [39]. Therefore, it can be concluded that most granitic dykes mainly originated from upper crustal melting. However, the strong depletion of Ti and P, as well as significant negative anomalies in Y and Yb, which formed in early-stage granite dykes, indicate that their sources were more likely to be derived from the melting of the lower crust and upper crust of the Bikou Group of the metamorphic volcanic basement, exhibiting characteristics of type I granites.

The granitic dykes exhibit δEu values ranging from 0.45 to 0.85, which indicate significant negative Eu anomalies. From their δEu values, the dykes can be separated into three groups, namely with values of 0.45–0.49 (five samples), 0.61–0.69 (six samples), and 0.70–0.85 (14 samples). Divalent Eu has the same ionic radius as Sr^{2+} and will be preferentially, over the trivalent REE, incorporated into calcic plagioclase and thus be rapidly depleted during fractional crystallization in the remaining melt.

During the initial stage of the Mianlue Ocean subduction collision, samples such as 21NS, 21PZB, 21SCKY, and 21BS03 fall within the I-type granite field, indicating that these samples possess I-type granite chemical characteristics (Figure 9d–e). However, due to the closure of the Mianlue Ocean, magma mixed with large amounts of crustal melt, causing samples such as 311-8, ZK1798, 21ZJS, and TC2101 to fall into the S-type granite field (Figure 9d). The feldspar or mica in these samples has been altered by hydrothermal fluids, as numerous feldspars observed under microscopic examination exhibit significant alteration to sericite, chlorite, and kaolinite, with visible feldspar remnants (Figure 4e,g). The water-rock interaction may be responsible for the extremely low Na content in these samples. Our samples indicate multi-stage and multi-period characteristics, pointing to a transition from syn-collisional or late-collisional to extensional environments. They demonstrate an evolution of granite types from I-type to S-type and then evolved into granite dykes with certain characteristics of A-type granite in the later stages.

During the inspection of thin sections under a petrographic microscope, small amounts of titanium-bearing minerals including ilmenite and titanite were found together with zircon and rutile in granite rock dykes. The samples collected were relatively fresh and unaltered. By utilizing major element and zirconium contents, we calculated the formation temperature of the granite dykes using a zircon saturation temperature thermometer [40]. Eight granitic rock samples (311-8-2, 311-2-4, 311-2-5, 311-2-8, 21ZJS03, 21ZJS04, 21ZJS05, and 21ZJS06) were formed between temperatures of 784 and 802 °C, possibly during the early stage of magmatic activity. Twelve additional granitic rock samples (ZK1798-2, ZK1798-3, ZK1798-4, 21NS02, 21NS03, 21NS04, 21PZB02, 21PZB03, 21XG02, 21XG03, and TC2101) were formed at an average temperature of 750 °C and temperatures ranging between 728 to 778 °C, indicating a time period of intense magmatic activity. Lastly, six fine-grained granite samples (21Scky02, 21Scky03, 21Scky04, 21BS02, and 21BS03) formed at temperatures ranging between 650 and 671 °C, which differs by more than 100 °C from the formation temperatures of other granite dykes, suggesting they were formed during the late stage of magmatic activity.

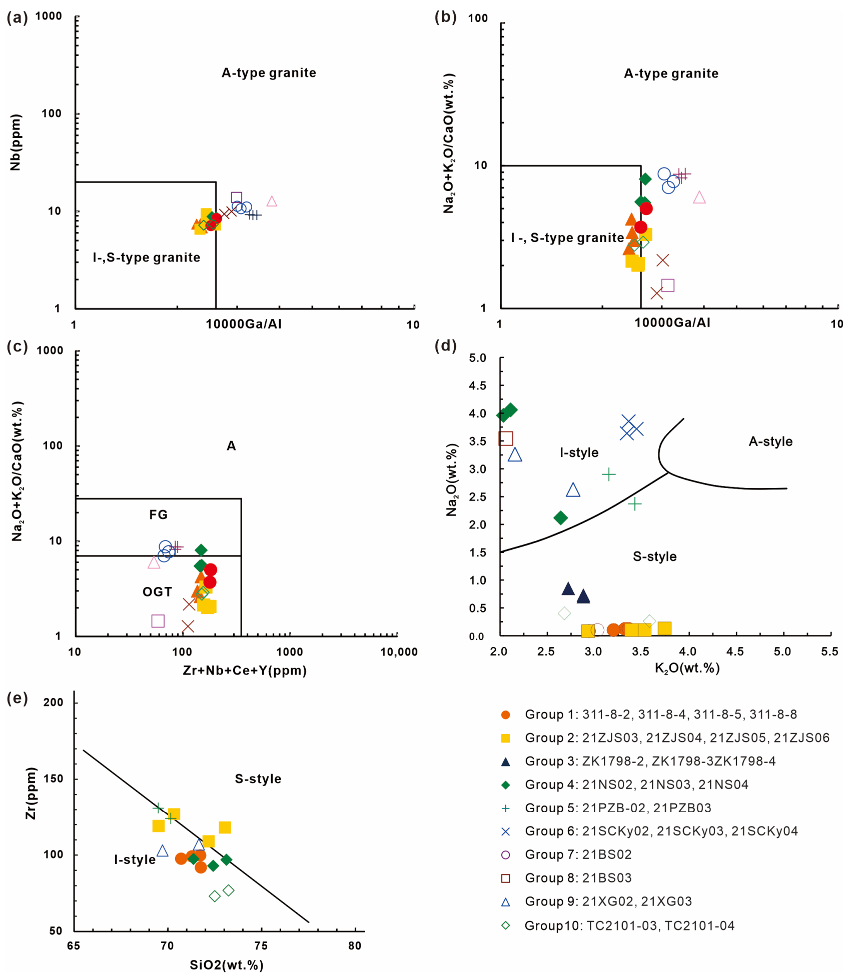

Figure 9. Discrimination diagrams of for the granitic dykes in the Yangshan gold belt [41,42]. (**a**) Nb(ppm) vs. 10000Ga/Al discrimination diagram; (**b**) ($Na_2O + K_2O$)/ CaO (wt.%) vs. 10000Ga/Al discrimination diagram; (**c**) (Na_2O + K_2O)/CaO (wt.%) vs. Zr + Nb + Ce + Y (ppm) discrimination diagram; (**d**) Na_2O (wt.%) vs. K_2O (wt.%) discrimination diagram; (**e**) Zr (ppm) vs. SiO_2 (wt.%) discrimination diagram. FG represents the differentiated felsic granite field; OGT represents undifferentiated S- and M-type granite fields.

In their study, Yang Guicai et al. (2016) [10] conducted isotopic analyses on granitic porphyry dykes in the Yangshan gold belt. They found that the origin of the granite can be traced back to collisionally thickened crustal material that underwent partial melting in the Bikou Group before being mixed with the Devonian lithologies during uplift. Our study has yielded similar results, but with some differences: the magma primarily originated from the less differentiated Bikou Group or Bikou Group metamorphosed volcanic basement, with some mixing from the Devonian surrounding rock. The dykes went through three stages of granite formation: I-type during the early stage, S-type during the middle stage, and granite with partial A-type characteristics during the late stage.

The Harker diagrams presented in Figure 10 illustrate that the concentrations of Ti, Fe, and P increase as the SiO_2 content increases. Conversely, when the SiO_2 content exceeds 76%, the values of Ti, Fe, and P in individual samples exhibit a decrease. Furthermore, Al, Ca, and Na + K demonstrate negligible changes with increasing SiO_2 content. These observations suggest that granitic dykes within the Yangshan gold belt display distinct evolutionary trends, which may result from different magmatic sources or wall rock compositions. Fractional crystallization is unlikely to be the dominant process of magmatic evolution, as evidenced by their different evolutionary trends on Harker diagrams (Figure 10) and discrimination diagrams (Figure 9).

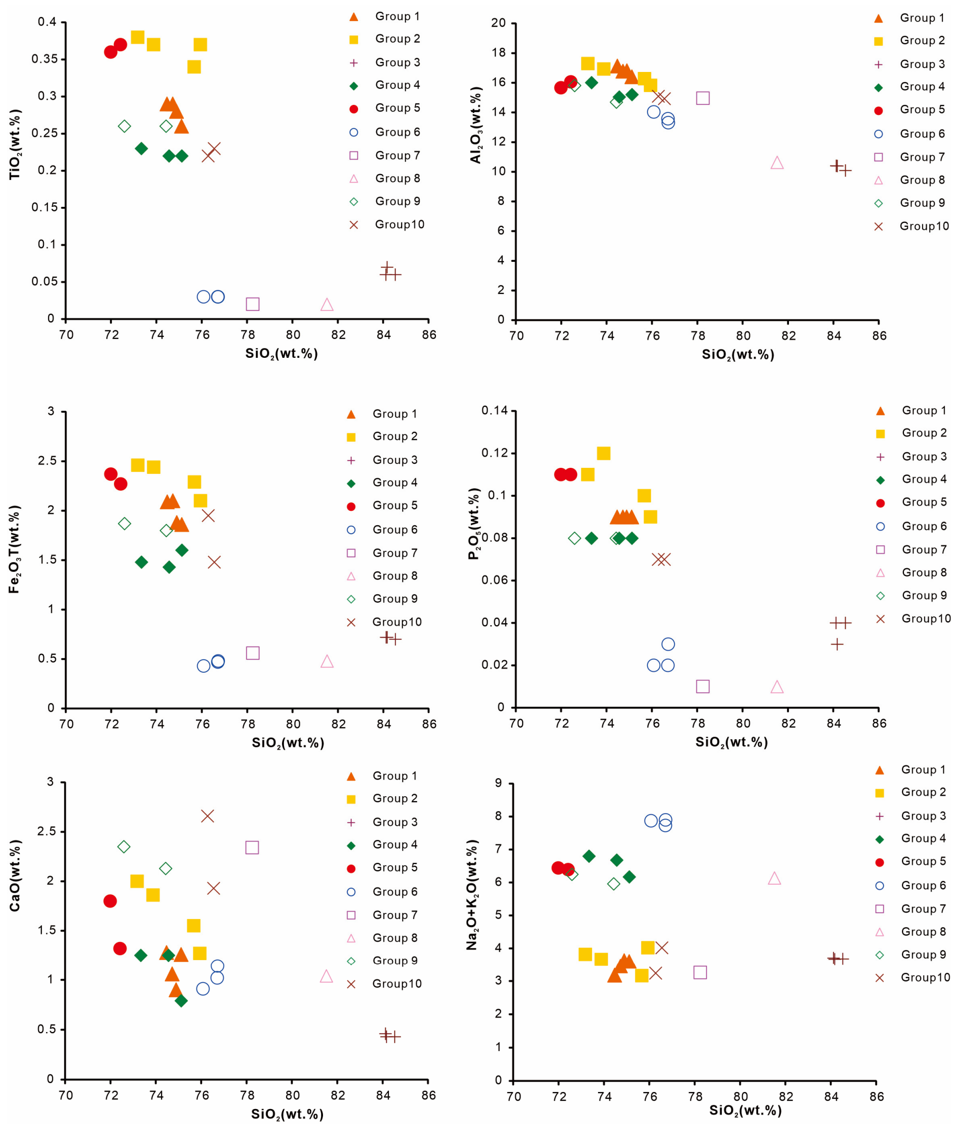

Figure 10. Harker diagrams of granite dykes in the Yangshan gold belt (refer to Figure 9 for legend).

Previous studies have shown that the P_2O_5 content varies insignificantly or not at all with SiO_2, indicating an S-type granitic character (Figure 10) [41–45]. Consistent with this, the P_2O_5 content of the 25 samples analyzed in this study vary insignificantly or not at all with SiO_2, further supporting their S-type granitic characteristics. It is hypothesized that the source of the granitic dykes originated from the melting of upper crustal sedimentary rocks or the incorporation of upper crustal materials. Subduction collision-induced crustal thickening and the addition of deep metamorphic water may be the key factors for upper crustal melting in this stage of the region.

In conclusion, the geochemical data presented in this study suggest that the Yangshan gold belt contains not only "S"-type granite dykes but also several "I"-type granite dykes, and some granite dykes show also "A"-type geochemical characteristics. These anomalies exhibit elemental geochemistry similar to A-type granite dykes, potentially influenced and modified by water-rock reactions.

5.2. Igneous Age

Table 4 presents geochronological results of nine granitic dykes, indicating that four contain inherited zircons, the ages of which are concentrated between 745.0 Ma and 802.0 Ma. This time frame matches the convergence and rifting of the Rodinia supercontinent as well as the subduction of the Yangtze plate, leading to extensive magmatism in the Bikou Terrane region. This event includes the Bikou Terrane (846–776 Ma) and sedimentary rocks (745–910 Ma) of the Bikou Group [46,47], alongside magmatic rocks in the Bikou Terrane [48–50]. Prior research indicates that significant magmatic activity occurred in and around the Mian-lue tectonic zone during the Neoproterozoic and Mesozoic eras. The chronology of granitic dykes in this study demonstrates that the granitic magmatic rocks in the Yangshan gold belt were primarily derived from the crustal base melting of the Bikou Group. During transport and emplacement, this melting was accompanied by the assimilation and mixing of ancient Mesozoic sedimentary layers, resulting in additional inherited zircon grains between 250 and 500 Ma in the granitic dykes.

In this study, previous research on granitic dykes in the Yangshan gold belt was reviewed to determine their age range (Table 5). The average age of these dykes was found to be 213.1 Ma, with a range between 177 Ma and 220.4 Ma [8,10,21,22]. The present study places the ages of the granite porphyry dykes between 201.0 Ma and 213 Ma, which is consistent with previous research. Among these dykes, the youngest ones are fine-grained granitic dykes and quartz porphyries, formed between 209 and 177 Ma [8,22]. In contrast, the medium- and coarse-grained granitic porphyries and tonalite porphyry dykes were mainly formed in the Late Triassic period, from 220 to 210 Ma, indicating a deeper environment which was beneficial for mineral growth during the early stages of formation. This contrasts with fine-grained granitic rocks and quartz porphyries, which were formed later during the process of collisional orogenic uplift, taking advantage of the early magma transport channels. The later igneous ages are mixed due to the use of earlier magma transport channels.

Our study found that the ages of granitic dykes in the Yangshan gold belt correlated with their proximity to the Wenxian arc tectonic zone. Dykes closer to this zone tend to be older, such as those found at Xinguan (223 Ma), Lianhecun (217–213 Ma), and Getiaowan (213–216 Ma). In contrast, dykes further away from the Wenxian arc zone tend to be younger, such as those found at Anba (209–215 Ma), Guanyinba (206 Ma), and Zhangjiashan (210 Ma). Zircon single-grain ages from the Yanshan period have even been observed in the granitic dykes of the Anba and Gejianwan sections.

This pattern is due to the location of the Yangshan gold belt in a tectonically weak zone controlled by the composite fracture zone of the Anchanghe-Guanyinba branch and the Getiaowan-Caopingliang complex backslope. The transition from an extrusional to an extensional-tensional environment provided a favorable transport channel for deep magma and late hydrothermal upwelling. During the Indosinian period, these tectonically weak zones led to the formation of granitic dykes intruded by fine-grained granite, and some of the Indosinian granite dykes were melted and assimilated by the heat of Yanshanian magma. This assimilation and mixing of the Indosinian and Yanshan magmas contributed to the age variations observed in the granitic dykes of the Yangshan gold belt.

Table 5. Results of dating granite dykes in the Yangshan gold belt.

No	Lithology	Sample No	Sampling Location	Age (Ma)	1σ	Analytical Method	Literature
1	Granite porphyry	LPD1	Lianhecun	217.8	2.8	SHRIMP Zircon U-Pb	[8]
2	Granite porphyry	LCK2	Lianhecun	212.7	3.4	SHRIMP Zircon U-Pb	
3	Fine-grained dykes	GCK1	Guojiapo	209.9	6.4	SHRIMP Zircon U-Pb	
4	Plagioclase granite porphyry	H01	Anba	215.9	3.1	SHRIMP Zircon U-Pb	
5	Plagioclase granite porphyry	TC439	Anba	115.8	1.6	SHRIMP Zircon U-Pb	
6	Quartz porphyry	ZK2596	Anba	209.6	1.6	SHRIMP Zircon U-Pb	
7	Plagioclase granite porphyry	N2	Nishan	207	3	SHRIMP Zircon U-Pb	
8	Granite porphyry	C01	Gaojiashan	211.1	1.8	Muscovite ^{40}Ar-^{39}Ar	[10]
9	Granite porphyry	14Y92	Gaojiashan	220.4	1.5	Muscovite ^{40}Ar-^{39}Ar	
10	Granite porphyry	AB01	Puzhiba	213.4	0.7	LA-ICPMS Zircon U-Pb	[21]
11	Granite porphyry	GTW02	Puzhiba	215.3	2.3	LA-ICPMS Zircon U-Pb	
12	Granite porphyry	AB02	Puzhiba	210.8	4	LA-ICPMS Zircon U-Pb	
13	Granite porphyry	GTW01	Puzhiba	213.3	0.6	LA-ICPMS Zircon U-Pb	
14	Granite porphyry	21PZB-1	Puzhiba	213.1	0.7	LA-ICPMS Zircon U-Pb	This article
15	Granite porphyry	21ZJS01	Puzhiba	210.49	76	LA-ICPMS Zircon U-Pb	
16	Ore-bearing quartz dykes	PD4-1	Anba	190.8	2.4	^{40}Ar-^{39}Ar Isochron age	[6]
17	Ore-bearing quartz dykes	YM	Anba	195.5– 200.9 126.9 51.2	 3.2 1.3	SHRIMP Zircon U-Pb	
18	Tonalite porphyry dykes	19GTW002	Getiaowan	216.5	2.4	LA-ICPMS Zircon U-Pb	[22]
19	Tonalite porphyry dykes	19GTW003	Getiaowan	214.8	1.2	LA-ICPMS Zircon U-Pb	
20	Fine-grained dykes	19GTW001	Getiaowan (YM621)	177.8	1.5	LA-ICPMS Zircon U-Pb	

5.3. Tectonic Evolution

We analyzed 25 samples of different lithologies from various sampling locations, which were distinguished into ten groups. The concentrations of major and trace elements were employed to differentiate the samples based on their tectonic position and petrogenetic type [51,52]. Figure 11a shows that the granitic porphyries consistently fall within the Slab failure field in the Nb-Y plot, while they form a cluster in the Syn-COLG and WPG ranges in the Ta-Yb plot (Figure 11b).

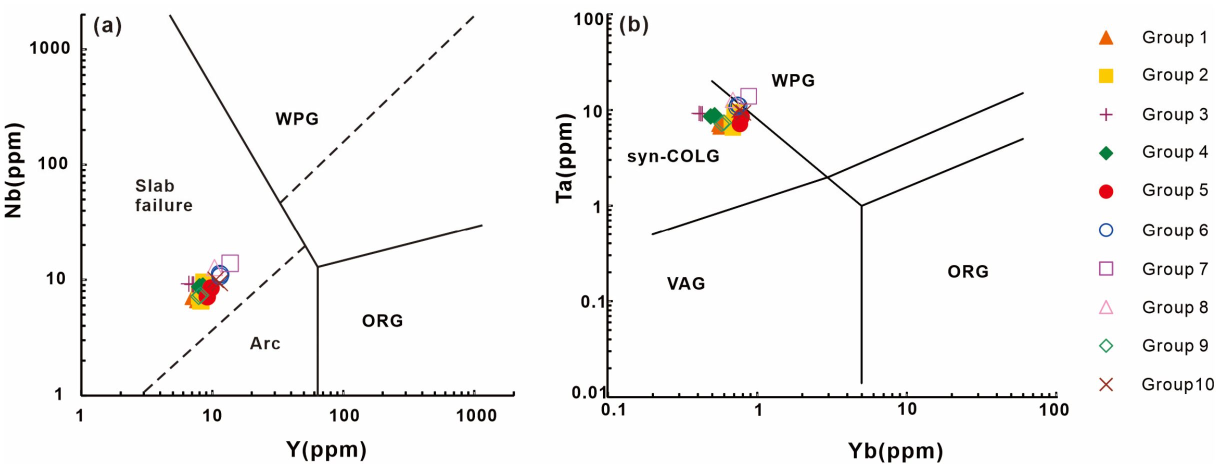

Figure 11. Illustration of tectonic setting of granite dykes in the Yangshan gold belt. ((**a**) according to Whalen et al., 2019 [51]; (**b**) according to Pearce et al., 1984 [52]). Abbreviations: WPG, within plate granite; syn-COLG, syn-collision granite; VAG, volcanic arc granite; ORG, ocean ridge granite.

Zou et al. (2022) [53] conducted a study on the granitic batholiths in the West Qinling ZeKu area and summarized previous chronological and geochemical data in the West Qinling region. Their findings suggest that the magmatic rocks in the West Qinling orogenic belt were formed due to the subduction collision of the Yangtze plate with the Qinling microplates and share a consistent origin and evolutionary history. These data indicate that the Paleo-Tethys Ocean experienced northward subduction at 264–225 Ma, followed by land-land syn-collision at 225–215 Ma, and then underwent a post-collision period beginning at 215 Ma.

Located in the western part of the Mian-lue suture zone, the Yangshan gold belt's age of the granitic dykes is concentrated between 220 and 200 Ma. This time frame is slightly later than that of the central portion of the Mian-lue suture zone due to the variation in the location of subduction collision between the Yangtze plate and the Qinling microplates. Therefore, the granitic dykes in this area share a similar geological background characterized by late collisional and post-collisional extrusion and extensional environments.

He et al. (2021) [50] examined granitic intrusions in the Bikou terrane and determined that they formed between 220 and 210 Ma in a post-collisional setting. Partial melting of the lower crust due to the injection of mafic magmas created felsic magma chambers that ultimately led to the development of Late Triassic granites found throughout the Bikou terrane. The geochemical characteristics of the granite intrusions indicate that the closure of the Mianlue Ocean caused the southwest escape of the Bikou terrane, resulting in weakened crust-mantle mixing and more mantle-derived materials being added to the northeastern Yangba pluton than to the southwestern margin of the Bikou terrane.

The granitic dykes are widely distributed in the study area. Based on zircon age, zircon Hf isotope analysis, and whole-rock major and trace element data of these dykes, it has been determined that they were generally formed during the Late Triassic period and are associated with the closure of the Mianlue Ocean, recording the features of Mianlue Ocean subduction collision with Qinling microplates and post-collision evolution. Combining previous research and the findings of this study, the age and tectonic geological background of the granitic dykes in the Yangshan gold belt can be divided into three stages (see Figure 12).

The first period was the subduction of the Mianlue Ocean that lasted from ~235–220 Ma (Figure 12a). At the end of this period, an oblique collision occurred between the two microplates from east to west, resulting in the Yangtze Plate's oceanic crust and subduction zone's accretionary wedge moving under the Qinling microplates. This movement caused some metamorphism in the lithosphere and mantle as well as the formation of mixtures of oceanic crust and upper crustal materials. These mixtures created medium- to coarse-grained granite dykes and bodies in the middle and deep crust with similar geochemical properties to I-type granites.

The second period, which lasted from ~220–210 Ma, was marked by the collision between the Yangtze Plate and the Qinling microplates (Figure 12b). During this period, the passive continental margin crust of the Yangtze Plate collided with the crust of the Qinling microplates, causing the rapid thickening of the Qinling microplates. The subducted plate ruptured, leading to large-scale heating and melting of the lower crust of the Qinling microplates. These melts mixed with some mafic upper mantle melts and formed a series of granite dykes and bodies along the tectonic weak zone. The granite intrusions accompanying the uplift of the Qinling microplates are medium- to fine-grained granite dykes, leaning mostly towards S-type granite characteristics.

The third period occurred from ~210–200 or 190 Ma and was characterized by post-collision continental extension (Figure 12c). During this period, the Yangtze Plate and Qinling microplates were in a geological background of strong compressive to extensional transition. Decompression melting of the upper crust took place, forming low-temperature granitic melts with high SiO_2 content. These melts quickly penetrated the surrounding rocks, forming medium- to coarse-grained granite dykes or medium-grained granite intrusions along previous magma transport channels that rapidly cooled to form fine- to very-fine-grained granite dykes. Although some of the geochemical characteristics of the granitic dykes match those of A-type granite, due to the collision-extension transition period, their melting temperature was lower, and the source area consisted mainly of partially melted upper crust, which is different from typical A-type granite characteristics.

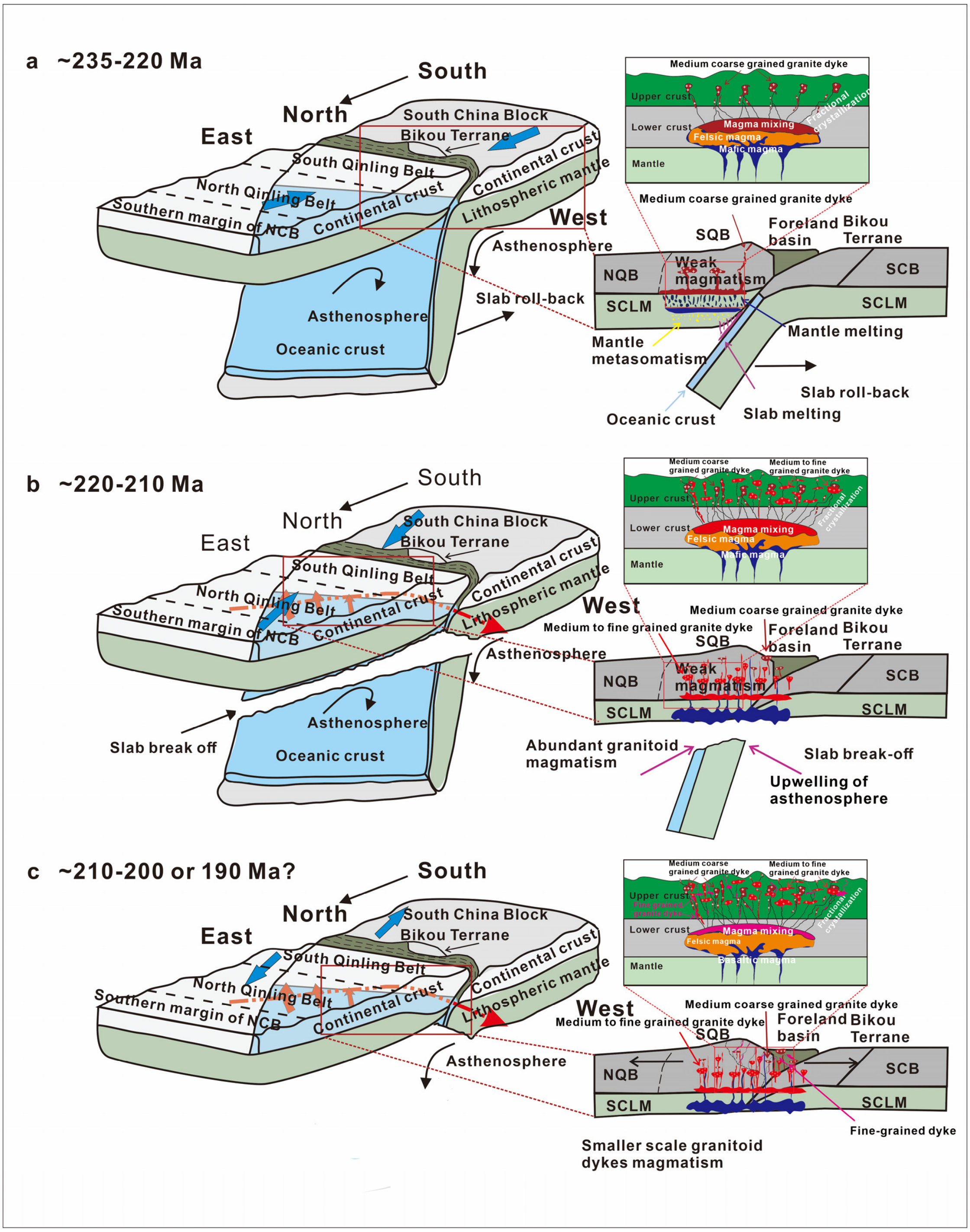

Figure 12. Schematic cartoon of the tectonic-magmatic evolution from 235 to 190 Ma in the Yangshan gold belt (modified according to [50]). (**a**) the subduction of the Mianlue Ocean that lasted from ~235–220 Ma; (**b**) the collision between the Yangtze Plate and the Qinling microplates from ~220–210 Ma; (**c**) the post-collision continental extension from ~210–200 or 190 Ma. NQB—North Qinling Blet, SQB—South Qinling Blet, NCB—North China Block, SCLM—Subcontinent lithospheric mantle.

The granitic dykes in the Yangshan gold belt were formed in a geological setting characterized by co-collisional extrusion after the subduction of the Yangtze plate beneath the Qinling microplates. The stretching occurred during the stage that followed the collisional shift to intraplate extension. The geochemical properties of the granitic dykes indicate the tectonic continuity of the collision in the Mian-Lue suture zone and its subsequent intraplate extension. Therefore, it can be concluded that the granitic dykes were formed in a geological environment that underwent subduction, co-collisional extrusion, and stretching.

5.4. Implications for the Genesis of Ore Deposits

The Yangshan gold belt hosts significant gold deposits, with the Yangshan deposit being the most notable with inferred resources of nearly 400 tons. However, there is ongoing debate over its genesis due to multiple tectonic changes and the effects of the Qinling orogeny. Orogenic, Carlin, and Carlin-like models are the dominant hypotheses, but their reconciliation is challenging. In our study, we have analyzed granitic dykes closely associated with mineralization to constrain the metallogenic age of the deposit. The previous ^{40}Ar-^{39}Ar dating of sericite/muscovite closely associated with gold obtained a mineralization age of 211–203 Ma [11]. Results show that the age of gold mineralization is consistent with the emplacement age of continental collision granitic dykes, which suggests that the metallogenic geological setting changed from subduction collision to the extension stage during the intracontinental orogenic period. Previous studies suggest that deep fluids or material and subduction zone accretionary wedge devolatilization might have contributed to the formation of orogenic gold deposits [54,55]. This paper proposes that deep material was transported along fractures to form gold ore bodies during the Yangshan gold belt transition from extrusion to extension. This scenario is in agreement with the geological background and characteristics of orogenic gold deposit formation.

6. Conclusions

(1) LA-ICP-MS zircon U-Pb dating results from granitic dykes reveal a concentration of inherited zircon ages, ranging from 745.0 Ma to 802.0 Ma, with some scattered Paleo-Mesozoic ages. This pattern suggests that the magma originated from basal melts of the Bikou Group and assimilated a modest proportion of surrounding rocks. The intrusion ages of this magmatic event cluster between 201.0 Ma and 213 Ma, indicating that the melts intruded during the late stage of collision between the Yangzte and Qinling microplates, marking the transition to an extensional environment.

(2) The granitic dykes have calc-alkaline to high-K calc-alkaline characteristics, are peraluminous, have moderate Eu anomalies (0.45–0.85), and are enriched in large-ion lithophile elements as well as Th and U, but are deficient in Ti and P. These granites are relatively enriched in light rare earth elements with (La/Yb) N ranging from 1.92 to 30.9 with a mean of 18.91) and relatively poor in heavy rare earth elements. We assign them as belonging to the late syn-collisional to post-collisional extensional environmental tectonic evolution.

(3) Major and trace element and Hf isotope analyses of the granitic dykes indicate that their source area was the volcanic rock basement of the Mesoproterozoic Bikou Group. During the thickening of the subducted Qinling microplate crust, the upper crust of the Bikou Group melted and migrated along the structurally weak zone, mixing and assimilating the surrounding rocks to form numerous granitic dykes. The tectonic and geological environment evolved from initial oceanic continental subduction to continental collision, ultimately transforming into intracontinental extension. The granite type also changed from the initial "I"-type to "S"-type, and finally evolved into granite with "A"-type characteristics.

Author Contributions: Conceptualization, Z.Y. and J.L.; Data curation, C.L. and W.W.; Formal analysis, Z.Y. and Y.H.; Investigation, Z.Y. and J.L.; Methodology, T.X. and Y.H.; Software, C.L. and Y.Z.; Writing—original draft, Z.Y.; Writing—review & editing, Z.Y. and J.L. All authors have read and agreed to the published version of the manuscript.

Funding: This research was funded by the Applied Geology Research Center of the China Geological Survey (No. DD20220971 and No. DD20191028).

Data Availability Statement: The data presented in this study are available in the Appendix A tables.

Acknowledgments: For assistance during fieldwork, we thank the Yangshan Project Team. The recommendations and advice of Li Jing Xiang were profitable in interpreting the data. We also thank the teachers in Wuhan Samplesolution and Guang-zhou for their help in the process of experiment and data processing. The modification suggestions and recommendations, which made by anonymous reviewers, have been of great help in improving and enhancing this article. We sincerely appreciate the efforts of the reviewers of this paper.

Conflicts of Interest: The authors declare no conflict of interest.

Appendix A

Table A1. Zircon LA-ICP-MS dating data of granite dykes in the Yangshan gold belt.

Measurement Points Number	^{232}Th	^{238}U	^{232}Th/U^{238}	Isotope Ratio									Isotope Age Values (Ma)							
	ppm	ppm		^{207}Pb/^{206}Pb	±2σ	^{207}Pb/^{235}U	±2σ	^{206}Pb/^{238}U	±2σ	^{208}Pb/^{232}Th	±2σ	^{238}U/^{232}Th	^{207}Pb/^{206}Pb	±2σ	^{207}Pb/^{235}U	±2σ	^{206}Pb/^{238}U	±2σ	^{208}Pb/^{232}Th	±2σ
21BS-001, Medium-Coarse-Grained Granite Dyke, Weighted Mean of 18 Points = 786.74 ± 1.88 ǀ 3.68 ǀ 20.58 Ma (n = 18/18) MSWD = 27.0, p(x2) = 0 (Excluding Points 04, 08, 18–23, 26–27, 29–30)																				
21BS-001-01	32	114	3.60	0.0704	0.0057	1.3190	0.1062	0.1363	0.0033	0.0432	0.0030	3.6799	940	167	854	47	824	19	855	58
21BS-001-02	89	98	1.10	0.0721	0.0070	1.3543	0.1226	0.1379	0.0047	0.0409	0.0023	1.1229	989	194	869	53	833	27	811	45
21BS-001-03	400	390	0.97	0.0673	0.0031	1.2633	0.0574	0.1361	0.0021	0.0423	0.0013	0.9921	856	97	829	26	823	12	837	24
21BS-001-04	401	400	1.00	0.1766	0.0055	11.6162	0.3598	0.4764	0.0067	0.1522	0.0038	1.0198	2621	52	2574	29	2511	29	2864	66
21BS-001-05	90	121	1.34	0.0667	0.0078	1.2487	0.1501	0.1357	0.0053	0.0395	0.0022	1.3702	829	246	823	68	820	30	783	44
21BS-001-06	122	78	0.64	0.0675	0.0076	1.1915	0.1230	0.1287	0.0044	0.0375	0.0020	0.6659	854	236	797	57	780	25	745	39
21BS-001-07	357	669	1.87	0.0663	0.0026	1.2389	0.0498	0.1353	0.0023	0.0400	0.0013	1.9089	817	82	818	23	818	13	793	25
21BS-001-08	222	305	1.37	0.1574	0.0047	9.3209	0.2695	0.4288	0.0066	0.1183	0.0032	1.4007	2429	50	2370	27	2300	30	2260	58
21BS-001-09	51	43	0.86	0.0633	0.0158	1.0580	0.2251	0.1250	0.0074	0.0376	0.0034	0.8772	718	552	733	111	759	42	746	67
21BS-001-10	206	169	0.82	0.0647	0.0048	1.0972	0.0814	0.1239	0.0031	0.0404	0.0019	0.8476	765	159	752	39	753	18	800	38
21BS-001-11	436	437	1.00	0.0646	0.0043	1.0763	0.0688	0.1210	0.0024	0.0372	0.0012	1.0264	761	143	742	34	736	14	738	23
21BS-001-12	556	290	0.52	0.0684	0.0068	1.1292	0.1077	0.1207	0.0045	0.0382	0.0015	0.5380	880	206	767	51	735	26	758	29
21BS-001-13	424	313	0.74	0.0692	0.0038	1.2011	0.0639	0.1260	0.0022	0.0407	0.0013	0.7685	906	113	801	29	765	13	807	25
21BS-001-14	97	152	1.58	0.0763	0.0058	1.3472	0.0983	0.1293	0.0031	0.0418	0.0021	1.6201	1102	152	866	43	784	18	828	40
21BS-001-15	287	227	0.79	0.0720	0.0049	1.1955	0.0856	0.1203	0.0032	0.0376	0.0014	0.8043	987	141	798	40	732	18	747	27
21BS-001-16	261	434	1.66	0.0660	0.0031	1.2699	0.0614	0.1392	0.0024	0.0434	0.0014	1.6774	807	98	832	27	840	14	860	27
21BS-001-17	346	595	1.72	0.0675	0.0029	1.2656	0.0545	0.1358	0.0026	0.0427	0.0015	1.7430	854	89	830	24	821	15	844	29
21BS-001-18	460	395	0.86	0.0567	0.0039	0.5266	0.0372	0.0673	0.0015	0.0209	0.0007	0.8686	480	158	430	25	420	9	418	14
21BS-001-19	1155	2012	1.74	0.0857	0.0026	2.6763	0.0858	0.2255	0.0036	0.0662	0.0018	1.7420	1331	59	1322	24	1311	19	1296	33
21BS-001-20	109	1664	15.28	0.0702	0.0022	1.4125	0.0460	0.1454	0.0022	0.0450	0.0019	15.7088	933	58	894	19	875	12	889	36
21BS-001-21	352	584	1.66	0.1774	0.0048	11.3687	0.3706	0.4620	0.0077	0.1269	0.0038	1.7285	2629	45	2554	30	2448	34	2416	68
21BS-001-22	525	856	1.63	0.0762	0.0044	1.0016	0.0574	0.0955	0.0016	0.0366	0.0015	1.6570	1100	111	705	29	588	9	727	30
21BS-001-23	1421	771	0.54	0.0815	0.0072	0.7681	0.0724	0.0676	0.0011	0.0246	0.0012	0.5685	1233	173	579	42	422	7	492	24
21BS-001-24	460	1023	2.23	0.0680	0.0025	1.2695	0.0491	0.1352	0.0022	0.0414	0.0013	2.2488	878	77	832	22	818	12	820	24
21BS-001-25	162	246	1.52	0.0683	0.0043	1.1377	0.0706	0.1214	0.0029	0.0400	0.0018	1.5868	880	130	771	34	739	17	793	35
21BS-001-26	455	626	1.37	0.1114	0.0034	4.9362	0.1615	0.3206	0.0053	0.0980	0.0025	1.3931	1833	54	1808	28	1793	26	1889	46
21BS-001-27	375	527	1.41	0.1203	0.0036	5.1598	0.1688	0.3105	0.0057	0.0997	0.0027	1.4582	1961	52	1846	28	1743	28	1920	49
21BS-001-28	563	455	0.81	0.0671	0.0036	1.1076	0.0569	0.1199	0.0020	0.0385	0.0013	0.8254	839	113	757	27	730	12	764	24
21BS-001-29	156	172	1.10	0.1196	0.0042	5.6253	0.2080	0.3406	0.0062	0.1010	0.0029	1.1217	1950	63	1920	32	1890	30	1946	54
21BS-001-30	563	1065	1.89	0.1628	0.0046	8.2868	0.2366	0.3681	0.0045	0.1109	0.0028	1.9321	2485	48	2263	26	2020	21	2125	51
21NS01, medium-coarse-grained plagioclase granite porphyry dyke, weighted mean of 14 points = 771.71 ± 1.88 ǀ 3.68 ǀ 17.56 Ma (n = 14/14) MSWD = 18.7,p(x2) = 0 (excluding points 01, 04–05, 8–9, 11, 13, 20, 22–23, 26)																				
21NS01-01	11	690	64.68	0.1105	0.0032	4.5682	0.1349	0.2990	0.0045	0.1077	0.0096	72.9624	1809	52	1743	25	1686	22	2068	176

Table A1. *Cont.*

Measurement Points Number	^{232}Th (ppm)	^{238}U (ppm)	$^{232}Th/U^{238}$	Isotope Ratio $^{207}Pb/^{206}Pb$	±2σ	$^{207}Pb/^{235}U$	±2σ	$^{206}Pb/^{238}U$	±2σ	$^{208}Pb/^{232}Th$	±2σ	$^{238}U/^{232}Th$	Isotope Age Values (Ma) $^{207}Pb/^{206}Pb$	±2σ	$^{207}Pb/^{235}U$	±2σ	$^{206}Pb/^{238}U$	±2σ	$^{208}Pb/^{232}Th$	±2σ
21NS01-02	166	201	1.21	0.0660	0.0050	1.0776	0.0817	0.1186	0.0025	0.0372	0.0014	1.2175	806	164	742	40	722	15	738	27
21NS01-03	150	193	1.28	0.0664	0.0044	1.1493	0.0787	0.1255	0.0031	0.0411	0.0019	1.3025	820	139	777	37	762	18	815	37
21NS01-04	176	348	1.98	0.1602	0.0047	9.5253	0.2845	0.4306	0.0064	0.1245	0.0034	2.0140	2457	49	2390	27	2308	29	2371	62
21NS01-05	468	519	1.11	0.0637	0.0037	0.8772	0.0568	0.0997	0.0033	0.0391	0.0010	1.1443	731	122	639	31	613	19	776	20
21NS01-06	444	462	1.04	0.0662	0.0029	1.0744	0.0486	0.1176	0.0021	0.0375	0.0011	1.0560	813	93	741	24	717	12	745	22
21NS01-07	202	265	1.32	0.0662	0.0036	1.2894	0.0716	0.1415	0.0030	0.0423	0.0015	1.3598	813	115	841	32	853	17	837	29
21NS01-08	240	510	2.13	0.1329	0.0040	5.2179	0.1779	0.2842	0.0063	0.0995	0.0027	2.2069	2136	52	1856	29	1612	32	1917	50
21NS01-09	867	324	0.37	0.1202	0.0040	6.0378	0.2121	0.3631	0.0063	0.1025	0.0027	0.3840	1959	60	1981	31	1997	30	1972	50
21NS01-10	287	243	0.85	0.0681	0.0039	1.2129	0.0694	0.1292	0.0025	0.0402	0.0014	0.8926	872	119	807	32	783	14	796	27
21NS01-11	1848	6499	3.52	0.3390	0.0107	1.6784	0.0657	0.0355	0.0006	0.1012	0.0037	3.6322	3658	48	1000	25	225	4	1948	69
21NS01-12	1674	745	0.45	0.0651	0.0025	1.1060	0.0413	0.1229	0.0017	0.0360	0.0008	0.4566	789	82	756	20	747	10	714	16
21NS01-13	423	1155	2.73	0.0911	0.0025	3.2758	0.0988	0.2602	0.0047	0.0752	0.0020	2.7744	1448	54	1475	23	1491	24	1466	38
21NS01-14	144	183	1.27	0.0676	0.0042	1.2345	0.0740	0.1330	0.0028	0.0412	0.0017	1.3086	857	130	816	34	805	16	817	33
21NS01-15	164	94	0.57	0.0713	0.0074	1.2286	0.1100	0.1285	0.0033	0.0403	0.0016	0.5916	966	213	814	50	779	19	798	31
21NS01-16	150	109	0.73	0.0693	0.0061	1.2662	0.1044	0.1356	0.0042	0.0416	0.0017	0.7849	907	179	831	47	820	24	824	33
21NS01-17	156	217	1.39	0.0680	0.0039	1.2448	0.0740	0.1329	0.0030	0.0397	0.0015	1.4179	878	121	821	33	804	17	787	29
21NS01-18	375	371	0.99	0.0686	0.0035	1.2169	0.0567	0.1293	0.0022	0.0388	0.0011	1.0547	887	106	808	26	784	12	769	21
21NS01-19	689	1078	1.57	0.0658	0.0023	1.2609	0.0504	0.1385	0.0026	0.0423	0.0013	1.6188	800	74	828	23	836	15	838	26
21NS01-20	340	340	1.00	0.0716	0.0039	1.2626	0.0646	0.1283	0.0023	0.0388	0.0012	1.0027	976	111	829	29	778	13	770	24
21NS01-21	987	839	0.85	0.0653	0.0024	1.1637	0.0442	0.1292	0.0021	0.0386	0.0011	0.8980	783	79	784	21	783	12	766	21
21NS01-22	1157	997	0.86	0.0703	0.0036	1.0614	0.0483	0.1101	0.0022	0.0366	0.0011	0.8780	939	105	735	24	673	13	727	22
21NS01-23	292	702	2.41	0.1094	0.0050	1.2053	0.0553	0.0808	0.0024	0.0550	0.0019	2.4153	1791	83	803	25	501	14	1083	36
21NS01-24	367	280	0.76	0.0685	0.0040	1.2515	0.0724	0.1330	0.0029	0.0407	0.0013	0.7841	885	122	824	33	805	17	806	25
21NS01-25	766	764	1.00	0.0676	0.0033	1.2298	0.0692	0.1312	0.0025	0.0402	0.0016	1.0205	857	106	814	32	794	14	796	31
21NS01-26	682	1545	2.27	0.2050	0.0119	1.3440	0.0506	0.0506	0.0028	0.0649	0.0023	2.5807	2878	94	865	22	318	17	1271	44
21PZB01, medium-coarse-grained plagioclase granite porphyry dyke, weighted mean of 15 points = 213.1 ± 0.7 | 1.6 Ma (n = 15/15) MSWD = 0.2, p(x2) = 1.0 (excluding points 01, 8–9, 11, 13, 15–16, 20, 23–25)																				
21PZB-01-01	314	270	0.86	0.0658	0.0045	1.1856	0.0792	0.1306	0.0033	0.0392	0.0017	0.8657	1200	144	794	37	791	19	778	33
21PZB-01-02	365	839	2.30	0.0504	0.0044	0.2338	0.0193	0.0336	0.0008	0.0109	0.0006	2.2433	213	254	213	16	213	5	219	13
21PZB-01-03	225	417	1.85	0.0526	0.0068	0.2405	0.0270	0.0337	0.0012	0.0108	0.0008	1.8840	322	261	219	22	214	8	216	17
21PZB-01-04	503	785	1.56	0.0527	0.0049	0.2435	0.0229	0.0337	0.0011	0.0109	0.0006	1.5451	317	208	221	19	214	7	219	13
21PZB-01-05	877	2743	3.13	0.0519	0.0038	0.2400	0.0188	0.0337	0.0014	0.0110	0.0007	3.0445	280	170	218	15	214	9	221	14
21PZB-01-06	515	703	1.37	0.0536	0.0074	0.2454	0.0315	0.0335	0.0013	0.0105	0.0006	1.3404	354	318	223	26	212	8	210	13
21PZB-01-07	318	810	2.55	0.0474	0.0051	0.2143	0.0216	0.0332	0.0009	0.0111	0.0008	2.4956	78	231	197	18	210	5	223	17
21PZB-01-08	1438	4925	3.42	0.6557	0.0226	9.4551	0.3431	0.1047	0.0027	0.5780	0.0186	3.4257	4637	50	2383	33	642	16	9220	238
21PZB-01-09	356	1135	3.18	0.2153	0.0321	0.9262	0.1214	0.0340	0.0022	0.0514	0.0070	2.7655	2945	242	666	64	215	14	1014	134
21PZB-01-10	524	1145	2.19	0.0523	0.0061	0.2394	0.0272	0.0334	0.0011	0.0116	0.0008	2.1419	298	268	218	22	212	7	233	15
21PZB-01-11	744	1025	1.38	0.0539	0.0050	0.2468	0.0211	0.0338	0.0009	0.0104	0.0006	1.4201	369	211	224	17	214	6	209	12

Table A1. *Cont.*

Measurement Points Number	^{232}Th (ppm)	^{238}U (ppm)	^{232}Th/U^{238}	Isotope Ratio ^{207}Pb/^{206}Pb	±2σ	^{207}Pb/^{235}U	±2σ	^{206}Pb/^{238}U	±2σ	^{208}Pb/^{232}Th	±2σ	^{238}U/^{232}Th	Isotope Age Values (Ma) ^{207}Pb/^{206}Pb	±2σ	^{207}Pb/^{235}U	±2σ	^{206}Pb/^{238}U	±2σ	^{208}Pb/^{232}Th	±2σ
21PZB-01-12	295	698	2.37	0.0531	0.0046	0.2968	0.0266	0.0404	0.0011	0.0133	0.0008	2.3291	332	200	264	21	255	7	268	17
21PZB-01-13	704	2952	4.19	0.0512	0.0031	0.2385	0.0149	0.0337	0.0007	0.0105	0.0005	4.1367	250	139	217	12	214	4	212	11
21PZB-01-14	2876	8107	2.82	0.6783	0.0209	9.0730	0.2838	0.0966	0.0015	0.4681	0.0208	2.8966	4687	47	2345	29	594	9	7761	286
21PZB-01-15	308	678	2.20	0.0538	0.0059	0.2473	0.0249	0.0339	0.0010	0.0108	0.0008	2.1651	365	248	224	20	215	6	218	15
21PZB-01-16	939	1424	1.52	0.0508	0.0039	0.2348	0.0185	0.0334	0.0007	0.0108	0.0005	1.5070	232	212	214	15	212	5	217	11
21PZB-01-17	1261	3660	2.90	0.2892	0.0248	1.7967	0.2031	0.0428	0.0029	0.0922	0.0099	2.9544	3414	135	1044	74	270	18	1782	184
21PZB-01-18	1147	3682	3.21	0.0509	0.0027	0.2379	0.0139	0.0337	0.0008	0.0107	0.0005	3.1667	235	124	217	11	214	5	215	10
21PZB-01-19	466	1581	3.39	0.1048	0.0148	0.5260	0.0748	0.0363	0.0009	0.0264	0.0026	3.3239	1710	258	429	50	230	5	526	52
21PZB-01-20	1204	4188	3.48	0.0500	0.0025	0.2337	0.0129	0.0337	0.0008	0.0106	0.0005	3.4269	195	114	213	11	214	5	214	9
21PZB-01-21	1084	2546	2.35	0.0549	0.0039	0.2546	0.0183	0.0335	0.0007	0.0111	0.0006	2.2905	409	161	230	15	213	4	223	12
21PZB-01-22	836	1549	1.85	0.0526	0.0048	0.2435	0.0225	0.0336	0.0008	0.0106	0.0006	1.8368	322	211	221	18	213	5	212	12
21PZB-01-23	325	278	0.86	0.0731	0.0050	1.3672	0.0969	0.1365	0.0038	0.0397	0.0017	0.8696	1017	140	875	42	825	22	787	33
21PZB-01-24	907	1435	1.58	0.0592	0.0049	0.2742	0.0215	0.0338	0.0008	0.0116	0.0005	1.5450	576	181	246	17	214	5	234	11
21PZB-01-25	631	1636	2.59	0.3592	0.0620	3.1434	0.5800	0.0633	0.0030	0.1370	0.0235	2.5126	3747	265	1443	142	396	18	2595	418

21XG01, medium and coarse grained granite porphyry dyke, weighted mean of 15 points = 801.97 ± 2.41 | 4.73 | 13.72 Ma (n = 10/11) MSWD = 6.32, p(c2) = 0.0000000053 (excluding points 01, 04, 8–9, 11, 13, 15–16, 20, 22–23, 26)

Measurement Points Number	^{232}Th (ppm)	^{238}U (ppm)	^{232}Th/U^{238}	Isotope Ratio ^{207}Pb/^{206}Pb	±2σ	^{207}Pb/^{235}U	±2σ	^{206}Pb/^{238}U	±2σ	^{208}Pb/^{232}Th	±2σ	^{238}U/^{232}Th	Isotope Age Values (Ma) ^{207}Pb/^{206}Pb	±2σ	^{207}Pb/^{235}U	±2σ	^{206}Pb/^{238}U	±2σ	^{208}Pb/^{232}Th	±2σ
21XG01-01	462	818	1.77	0.1114	0.0040	2.7524	0.1561	0.1789	0.0082	0.0755	0.0025	1.8671	1822	59	1343	42	1061	45	1472	47
21XG01-02	172	237	1.38	0.0697	0.0041	1.2972	0.0746	0.1355	0.0028	0.0440	0.0016	1.4200	920	121	844	33	819	16	870	32
21XG01-03	251	382	1.52	0.0709	0.0030	1.3060	0.0585	0.1339	0.0029	0.0453	0.0018	1.5545	954	87	848	26	810	17	895	35
21XG01-04	169	260	1.54	0.0688	0.0042	1.1292	0.0685	0.1192	0.0026	0.0415	0.0019	1.5981	894	128	767	33	726	15	823	37
21XG01-05	93	148	1.60	0.0687	0.0056	1.1662	0.0916	0.1251	0.0033	0.0405	0.0023	1.6364	889	170	785	43	760	19	802	45
21XG01-06	307	899	2.93	0.1064	0.0041	4.1601	0.1715	0.2839	0.0071	0.0889	0.0028	2.9870	1739	65	1666	34	1611	36	1721	53
21XG01-07	281	391	1.39	0.0687	0.0034	1.2303	0.0658	0.1296	0.0024	0.0401	0.0014	1.4052	889	103	814	30	786	14	794	27
21XG01-08	1115	769	0.69	0.0578	0.0027	0.6596	0.0301	0.0831	0.0014	0.0256	0.0007	0.7030	520	102	514	18	515	9	510	13
21XG01-09	1092	1091	1.00	0.0705	0.0022	1.3091	0.0393	0.1348	0.0020	0.0438	0.0010	1.0406	944	65	850	17	815	11	866	19
21XG01-10	218	231	1.06	0.0720	0.0048	1.2931	0.0885	0.1306	0.0032	0.0410	0.0015	1.0411	987	131	843	39	791	18	811	30
21XG01-11	352	1906	5.41	0.1044	0.0084	0.6029	0.0605	0.0402	0.0014	0.0644	0.0102	7.2929	1706	154	479	38	254	9	1262	193
21XG01-12	212	314	1.48	0.0692	0.0046	1.2953	0.0946	0.1349	0.0026	0.0450	0.0024	1.4978	906	137	844	42	816	15	889	46
21XG01-13	77	101	1.31	0.0709	0.0066	1.2636	0.1155	0.1307	0.0034	0.0437	0.0023	1.3239	954	197	830	52	792	19	864	45
21XG01-14	1119	1568	1.40	0.0840	0.0040	0.7372	0.0339	0.0639	0.0014	0.0296	0.0010	1.4624	1292	94	561	20	400	8	590	20
21XG01-15	1154	1760	1.53	0.1888	0.0180	3.0808	0.3286	0.1149	0.0020	0.0964	0.0103	1.5795	2732	158	1428	82	701	12	1861	190
21XG01-16	218	421	1.93	0.0698	0.0034	1.3971	0.0635	0.1457	0.0027	0.0457	0.0017	1.9954	924	100	888	27	877	15	903	32
21XG01-17	699	1181	1.69	0.0887	0.0026	2.8877	0.0934	0.2356	0.0047	0.0705	0.0018	1.6852	1398	57	1379	24	1364	24	1378	34
21XG01-18	1036	1302	1.26	0.1287	0.0042	6.4428	0.2404	0.3611	0.0071	0.1080	0.0036	1.2907	2080	57	2038	33	1987	33	2074	66
21XG01-19	341	715	2.09	0.2378	0.0066	17.0316	0.4833	0.5171	0.0072	0.1505	0.0038	2.1631	3105	44	2937	27	2687	30	2833	66
21XG01-20	30	8	0.27	1.2853	0.3021	327.1028	217.0599	2.5676	2.4375	6.5424	5.7793	0.0242	error	error	5882	672	8199	4404	40,840	15,487
21XG01-21	132	140	1.06	0.0749	0.0070	1.2925	0.1130	0.1264	0.0037	0.0429	0.0021	1.0833	1065	189	842	50	767	21	849	40

Table A1. *Cont.*

Measurement Points Number	^{232}Th	^{238}U	^{232}Th/U^{238}	Isotope Ratio									Isotope Age Values (Ma)							
	ppm			^{207}Pb/^{206}Pb	±2σ	^{207}Pb/^{235}U	±2σ	^{206}Pb/^{238}U	±2σ	^{208}Pb/^{232}Th	±2σ	^{238}U/^{232}Th	^{207}Pb/^{206}Pb	±2σ	^{207}Pb/^{235}U	±2σ	^{206}Pb/^{238}U	±2σ	^{208}Pb/^{232}Th	±2σ
21XG01-22	1065	1393	1.31	0.1416	0.0046	3.0215	0.0997	0.1540	0.0020	0.0802	0.0021	1.3250	2247	56	1413	25	923	11	1559	39
21XG01-23	350	517	1.48	0.2916	0.0345	5.0647	0.7407	0.1224	0.0053	0.1516	0.0218	1.5562	3428	185	1830	124	744	31	2853	382
21XG01-24	387	1746	4.51	0.0792	0.0038	0.3759	0.0171	0.0344	0.0006	0.0219	0.0014	5.2229	1177	99	324	13	218	4	438	28
21XG01-25	496	555	1.12	0.0700	0.0034	1.2716	0.0585	0.1319	0.0022	0.0403	0.0013	1.1344	929	97	833	26	799	12	799	25
21XG01-26	577	1044	1.81	0.1712	0.0145	1.8142	0.1498	0.0853	0.0054	0.0648	0.0037	1.8967	2569	143	1051	54	528	32	1269	70
21XG01-27	710	3303	4.65	0.0853	0.0047	0.4017	0.0226	0.0341	0.0006	0.0242	0.0015	4.7166	1321	108	343	16	216	4	483	30
21XG01-28	270	284	1.05	0.1330594	0.012924	2.6933343	0.3247097	0.1377843	0.0040984	0.0675153	0.0062739	1.0716061	2139	171	1327	89	832	23	1321	119
21XG01-29	741	1451	1.96	0.0812092	0.0029326	1.3104955	0.0460247	0.1169928	0.0019524	0.0476113	0.002047	2.0046696	1228	71	850	20	713	11	940	39
21ZJS01, medium-coarse-grained granite dyke, weighted mean of 8 points = 210.49 ± 0.76 | 1.50 Ma (n = 8/8) MSWD = 1.34, p(c2) = 0.23 (excluding points 01, 05, 7–16, 19–20, 23–26)																				
21ZJS01-01	135	184	1.36	0.0728	0.0040	1.3604	0.0721	0.1365	0.0030	0.0438	0.0017	1.3852	1007	108	872	31	825	17	867	33
21ZJS01-02	172	390	2.27	0.0470	0.0054	0.2168	0.0228	0.0339	0.0009	0.0114	0.0007	2.3338	50	252	199	19	215	6	229	13
21ZJS01-03	766	1152	1.50	0.0477	0.0027	0.2162	0.0121	0.0330	0.0006	0.0101	0.0004	1.5446	87	130	199	10	209	4	204	8
21ZJS01-04	229	513	2.24	0.0524	0.0048	0.2337	0.0214	0.0325	0.0008	0.0105	0.0006	2.3039	302	207	213	18	206	5	212	12
21ZJS01-05	243	900	3.70	0.0992	0.0063	0.4243	0.0251	0.0312	0.0008	0.0241	0.0011	3.7701	1610	118	359	18	198	5	482	21
21ZJS01-06	279	385	1.38	0.0538	0.0050	0.2434	0.0213	0.0330	0.0008	0.0105	0.0005	1.4024	361	211	221	17	209	5	211	10
21ZJS01-07	251	246	0.98	0.0687	0.0036	1.2368	0.0634	0.1309	0.0026	0.0400	0.0015	0.9920	900	103	817	29	793	15	793	28
21ZJS01-08	446	1853	4.15	0.1147	0.0070	0.4430	0.0250	0.0282	0.0005	0.0273	0.0015	4.3160	1876	111	372	18	179	3	545	30
21ZJS01-09	308	761	2.47	0.0773	0.0041	0.3896	0.0191	0.0368	0.0008	0.0167	0.0008	2.5175	1131	106	334	14	233	5	335	15
21ZJS01-10	395	588	1.49	0.0896	0.0043	1.0135	0.0498	0.0821	0.0021	0.0432	0.0015	1.6198	1417	93	711	25	509	13	855	29
21ZJS01-11	716	2910	4.06	0.1096	0.0103	0.4242	0.0388	0.0284	0.0005	0.0257	0.0025	4.0454	1792	172	359	28	180	3	513	50
21ZJS01-12	290	190	0.66	0.0705	0.0048	1.1978	0.0811	0.1239	0.0029	0.0395	0.0013	0.6695	944	141	800	37	753	17	783	25
21ZJS01-13	381	443	1.16	0.0637	0.0035	1.0667	0.0595	0.1217	0.0027	0.0378	0.0012	1.1898	731	123	737	29	740	15	750	24
21ZJS01-14	307	374	1.22	0.0652	0.0039	1.1779	0.0796	0.1307	0.0035	0.0416	0.0018	1.2260	789	126	790	37	792	20	825	34
21ZJS01-15	60	332	5.56	0.0553	0.0053	0.2848	0.0263	0.0375	0.0009	0.0199	0.0017	5.8065	433	218	254	21	238	6	399	34
21ZJS01-16	418	675	1.61	0.0645	0.0024	1.1678	0.0429	0.1313	0.0022	0.0406	0.0012	1.6356	767	80	786	20	795	13	804	23
21ZJS01-17	593	1071	1.81	0.0530	0.0036	0.2448	0.0171	0.0333	0.0007	0.0107	0.0004	1.8392	328	154	222	14	211	4	214	8
21ZJS01-18	486	825	1.70	0.0519	0.0041	0.2334	0.0175	0.0328	0.0007	0.0104	0.0005	1.7764	283	177	213	14	208	4	210	10
21ZJS01-19	684	1975	2.89	0.1050	0.0045	0.5362	0.0219	0.0370	0.0006	0.0302	0.0011	2.9707	1714	79	436	14	234	4	601	22
21ZJS01-20	319	219	0.69	0.0701	0.0045	1.2119	0.0804	0.1252	0.0030	0.0388	0.0013	0.6846	932	132	806	37	760	17	768	26
21ZJS01-21	627	1702	2.71	0.0503	0.0026	0.2325	0.0115	0.0335	0.0006	0.0102	0.0004	2.7219	209	119	212	9	212	4	205	7
21ZJS01-22	418	1480	3.54	0.0511	0.0033	0.2361	0.0152	0.0335	0.0006	0.0114	0.0006	3.7582	256	144	215	12	212	4	228	12
21ZJS01-23	665	2385	3.59	0.2274	0.0147	1.5664	0.1430	0.0476	0.0022	0.1112	0.0113	4.0409	3035	103	957	57	299	13	2131	205
21ZJS01-24	349	612	1.75	0.0595	0.0049	0.2689	0.0232	0.0327	0.0007	0.0113	0.0007	1.8027	585	180	242	19	207	4	227	14
21ZJS01-25	753	1875	2.49	0.1357	0.0130	0.5715	0.0478	0.0315	0.0010	0.0270	0.0021	2.7753	2173	168	459	31	200	6	538	41
21ZJS01-26	264	252	0.95	0.0643	0.0038	1.0738	0.0640	0.1214	0.0030	0.0382	0.0012	0.9533	752	119	741	31	739	17	758	24
311-8-1, granite porphyry dyke, weighted mean of 2 points = 213.3 ± 7 Ma (n = 2/2)																				
311-8-1-01	147	213	1.44	0.0722	0.0067	1.2775	0.1214	0.1293	0.0053	0.0427	0.0026	1.4319	992	190	836	54	784	30	845	50

Table A1. *Cont.*

Measurement Points Number	^{232}Th	^{238}U	^{232}Th/U^{238}	Isotope Ratio									Isotope Age Values (Ma)							
	ppm			^{207}Pb/^{206}Pb	±2σ	^{207}Pb/^{235}U	±2σ	^{206}Pb/^{238}U	±2σ	^{208}Pb/^{232}Th	±2σ	^{238}U/^{232}Th	^{207}Pb/^{206}Pb	±2σ	^{207}Pb/^{235}U	±2σ	^{206}Pb/^{238}U	±2σ	^{208}Pb/^{232}Th	±2σ
311-8-1-02	516	1249	2.42	0.0546	0.0035	0.4433	0.0276	0.0590	0.0012	0.0182	0.0008	2.4634	394	138	373	19	369	7	365	17
311-8-1-03	113	265	2.34	0.0748	0.0071	1.3168	0.1331	0.1293	0.0069	0.0459	0.0031	2.4258	1065	191	853	58	784	39	908	60
311-8-1-04	703	1312	1.87	0.0528	0.0033	0.4071	0.0268	0.0559	0.0016	0.0185	0.0011	2.0765	320	143	347	19	351	10	371	21
311-8-1-05	838	2506	2.99	0.1039	0.0105	0.3948	0.0270	0.0303	0.0017	0.0226	0.0014	3.0172	1695	188	338	20	193	10	452	28
311-8-1-06	656	511	0.78	0.0652	0.0050	0.9942	0.0773	0.1113	0.0039	0.0356	0.0018	0.7923	783	194	701	39	680	22	706	35
311-8-1-07	1516	4228	2.79	0.1143	0.0213	0.5500	0.1866	0.0319	0.0038	0.0301	0.0089	2.9485	1869	342	445	122	203	24	599	174
311-8-1-08	454	830	1.83	0.0772	0.0078	0.5073	0.0510	0.0480	0.0015	0.0245	0.0022	2.7009	1126	202	417	34	302	9	489	43
311-8-1-09	958	1637	1.71	0.0547	0.0038	0.4052	0.0325	0.0534	0.0015	0.0178	0.0011	2.1314	467	156	345	23	335	9	357	21
311-8-1-10	257	633	2.46	0.0641	0.0040	1.1376	0.0692	0.1293	0.0031	0.0421	0.0022	2.4999	746	131	771	33	784	17	834	42
311-8-1-11	4027	2223	0.55	0.1346	0.0068	2.9594	0.1545	0.1604	0.0056	0.0629	0.0027	0.6064	2159	88	1397	40	959	31	1233	50
311-8-1-12	1837	4025	2.19	0.0554	0.0054	0.2315	0.0234	0.0303	0.0008	0.0102	0.0006	2.2163	428	218	211	19	192	5	205	11
311-8-1-13	384	881	2.30	0.0738	0.0037	1.6709	0.0839	0.1641	0.0035	0.0516	0.0020	2.3327	1037	72	998	32	980	19	1017	39
311-8-1-14	1149	1588	1.38	0.0552	0.0036	0.3904	0.0265	0.0514	0.0014	0.0167	0.0008	1.6599	420	151	335	19	323	8	335	16
311-8-1-15	361	747	2.07	0.0636	0.0101	0.4600	0.0830	0.0515	0.0017	0.0201	0.0031	2.1785	728	341	384	58	324	10	403	61
311-8-1-16	959	1528	1.59	0.0508	0.0037	0.3537	0.0237	0.0507	0.0014	0.0161	0.0007	1.6571	232	168	308	18	319	8	323	14
311-8-1-17	1406	3256	2.32	0.0531	0.0036	0.2360	0.0162	0.0322	0.0009	0.0111	0.0006	2.5393	345	157	215	13	204	6	224	13
311-8-1-18	994	2776	2.79	0.1188	0.0152	0.5345	0.0663	0.0330	0.0011	0.0267	0.0034	2.9192	1939	225	435	44	209	7	532	67
311-8-1-19	813	579	0.71	0.0777	0.0054	1.2096	0.0772	0.1129	0.0023	0.0372	0.0016	0.7750	1140	140	805	35	690	13	739	32
311-8-1-20	1051	3327	3.16	0.1437	0.0270	0.8838	0.3201	0.0396	0.0086	0.1492	0.0858	4.8384	2272	330	643	173	250	53	2812	1508
311-8-1-21	3150	7159	2.27	0.3416	0.0987	11.8696	7.0877	0.1247	0.0476	0.3979	0.1924	4.3299	3670	457	2594	559	757	273	6771	2782
311-8-1-22	1297	3318	2.56	0.0833	0.0132	0.4541	0.1112	0.0362	0.0036	0.0177	0.0028	2.5168	1276	314	380	78	229	22	356	56
311-8-6, granite porphyry dyke, weighted mean of 11 points = 749.89 ± 2.48 | 4.86 | 38.91 Ma (n = 11/11) MSWD = 49.6, p(c2) = 0 (excluding points 01, 05, 7–16, 19–20, 23–25)																				
311-8-6-01	196	697	3.56	0.1257	0.0037	6.2044	0.1968	0.3564	0.0059	0.1049	0.0035	3.6155	2039	56	2005	28	1965	28	2016	64
311-8-6-02	56	78	1.39	0.0690	0.0075	1.2336	0.1285	0.1318	0.0038	0.0414	0.0026	1.4129	898	228	816	58	798	22	820	50
311-8-6-03	273	541	1.98	0.0688	0.0029	1.3224	0.0535	0.1394	0.0025	0.0432	0.0013	2.0041	894	85	856	23	842	14	854	26
311-8-6-04	179	164	0.91	0.0657	0.0051	1.0807	0.0806	0.1203	0.0029	0.0362	0.0014	0.9326	798	162	744	39	732	17	720	28
311-8-6-05	426	437	1.03	0.0657	0.0035	1.0852	0.0600	0.1204	0.0035	0.0379	0.0012	1.0600	798	111	746	29	733	20	752	23
311-8-6-06	1666	2142	1.29	0.1594	0.0064	1.5539	0.0629	0.0707	0.0015	0.0461	0.0014	1.3412	2449	68	952	25	440	9	911	26
311-8-6-07	1502	3456	2.30	0.1654	0.0090	0.8557	0.0455	0.0375	0.0006	0.0351	0.0016	2.3516	2522	97	628	25	237	4	698	31
311-8-6-08	345	389	1.13	0.0689	0.0038	1.0451	0.0566	0.1103	0.0023	0.0378	0.0012	1.1833	896	115	726	28	675	14	750	23
311-8-6-09	257	202	0.79	0.0646	0.0052	0.9534	0.0722	0.1078	0.0026	0.0383	0.0011	0.8199	761	169	680	38	660	15	759	22
311-8-6-10	604	495	0.82	0.1104	0.0031	4.7032	0.1375	0.3075	0.0043	0.0889	0.0021	0.8354	1806	52	1768	25	1728	21	1721	38
311-8-6-11	544	481	0.88	0.0663	0.0026	1.2062	0.0461	0.1316	0.0023	0.0406	0.0011	0.8993	817	81	803	21	797	13	803	22
311-8-6-12	1564	6107	3.91	0.1088	0.0057	0.3804	0.0183	0.0256	0.0006	0.0217	0.0011	4.3465	1789	96	327	13	163	4	434	21
311-8-6-13	224	183	0.82	0.0663	0.0081	1.0104	0.1085	0.1118	0.0042	0.0362	0.0019	0.8293	815	225	709	55	683	24	719	38
311-8-6-14	809	956	1.18	0.1801	0.0140	1.7571	0.0814	0.0776	0.0040	0.0677	0.0052	1.3993	2653	129	1030	30	482	24	1324	99
311-8-6-15	861	1149	1.33	0.0786	0.0029	1.3231	0.0420	0.1226	0.0023	0.0445	0.0010	1.3643	1162	73	856	18	745	13	880	20
311-8-6-16	292	272	0.93	0.0741	0.0057	1.3763	0.0978	0.1354	0.0034	0.0442	0.0019	0.9467	1044	155	879	42	819	19	874	36

Table A1. *Cont.*

Measurement Points Number	^{232}Th	^{238}U	^{232}Th/U^{238}	Isotope Ratio									Isotope Age Values (Ma)							
	ppm			^{207}Pb/^{206}Pb	±2σ	^{207}Pb/^{235}U	±2σ	^{206}Pb/^{238}U	±2σ	^{208}Pb/^{232}Th	±2σ	^{238}U/^{232}Th	^{207}Pb/^{206}Pb	±2σ	^{207}Pb/^{235}U	±2σ	^{206}Pb/^{238}U	±2σ	^{208}Pb/^{232}Th	±2σ
311-8-6-17	569	843	1.48	0.0651	0.0030	1.1611	0.0534	0.1290	0.0022	0.0386	0.0011	1.5073	789	96	782	25	782	12	765	21
311-8-6-18	288	405	1.41	0.0863	0.0051	1.2211	0.0653	0.1045	0.0034	0.0457	0.0014	1.4054	1346	113	810	30	641	20	904	28
311-8-6-19	193	246	1.27	0.0690	0.0046	1.1864	0.0729	0.1263	0.0030	0.0425	0.0016	1.3065	898	138	794	34	767	17	840	31
311-8-6-20	690	981	1.42	0.1803	0.0189	1.0076	0.0664	0.0449	0.0018	0.0393	0.0032	1.5788	2655	174	708	34	283	11	778	61
311-8-6-21	490	600	1.22	0.0749	0.0039	1.1728	0.0738	0.1133	0.0046	0.0382	0.0012	1.2370	1066	101	788	34	692	27	757	24
311-8-6-22	646	2029	3.14	0.1230	0.0089	0.7062	0.0359	0.0429	0.0012	0.0414	0.0015	3.1861	2000	129	542	21	271	7	821	29
311-8-6-23	404	1048	2.59	0.1666	0.0078	1.1094	0.0564	0.0495	0.0024	0.0576	0.0022	2.5131	2523	78	758	27	311	15	1132	41
311-8-6-24	672	1035	1.54	0.0699	0.0034	0.8262	0.0492	0.0847	0.0027	0.0330	0.0014	1.5759	926	106	612	27	524	16	656	27
311-8-6-25	303	490	1.62	0.1446	0.0160	1.1762	0.0774	0.0712	0.0059	0.0511	0.0032	1.7881	2284	191	790	36	443	36	1008	62
311-8-6-26	179	124	0.69	0.0722	0.0055	1.3312	0.0982	0.1356	0.0041	0.0447	0.0019	0.7098	991	156	859	43	820	24	884	36
311-8-6-27	350	591	1.69	0.1598	0.0044	9.4185	0.2772	0.4261	0.0071	0.1197	0.0030	1.7429	2454	48	2380	27	2288	32	2286	53
TC2101-02, granite porphyry dyke, 3-site weighted mean = 206.7 ± 1.2 | 2.8 | 31.5 Ma (n = 3) MSWD = 14, p(c2) = 0.000001 (contains 15, 21, 29)																				
TC2101-02-01	3442	14,607	4.24	0.5315	0.0132	2.0360	0.0575	0.0276	0.0004	0.1496	0.0037	4.2510	4331	36	1128	19	176	2	2819	65
TC2101-02-02	5551	22,583	4.07	0.3694	0.0085	0.6031	0.0164	0.0118	0.0002	0.0428	0.0012	4.1257	3791	35	479	10	76	1	847	24
TC2101-02-03	1211	7025	5.80	0.1479	0.0052	0.5342	0.0156	0.0265	0.0008	0.0452	0.0011	5.8915	2321	59	435	10	169	5	893	22
TC2101-02-04	901	6952	7.72	0.3156	0.0143	1.4485	0.0452	0.0340	0.0009	0.1832	0.0056	7.7910	3550	70	909	19	215	6	3401	95
TC2101-02-05	8095	25,620	3.17	0.4946	0.0130	0.8437	0.0242	0.0123	0.0002	0.0468	0.0013	3.2061	4225	39	621	13	79	1	925	25
TC2101-02-06	5372	17,561	3.27	0.4456	0.0104	1.2623	0.0378	0.0205	0.0005	0.0725	0.0021	3.3213	4072	35	829	17	131	3	1414	39
TC2101-02-07	6926	17,735	2.56	0.3402	0.0076	0.7789	0.0225	0.0165	0.0003	0.0351	0.0010	2.6175	3664	34	585	13	106	2	697	20
TC2101-02-08	5489	20,271	3.69	0.3665	0.0095	0.7633	0.0201	0.0152	0.0004	0.0490	0.0014	3.8432	3777	38	576	12	97	2	968	26
TC2101-02-09	5538	20,673	3.73	0.5281	0.0125	1.2432	0.0280	0.0171	0.0003	0.0832	0.0021	3.9037	4322	40	820	13	109	2	1616	39
TC2101-02-10	271	586	2.16	0.0640	0.0033	0.8040	0.0416	0.0910	0.0015	0.0360	0.0013	2.2990	743	111	599	23	562	9	715	25
TC2101-02-11	6864	18,392	2.68	0.2627	0.0078	0.4613	0.0141	0.0127	0.0002	0.0208	0.0006	2.7612	3265	46	385	10	81	1	417	11
TC2101-02-12	1167	3709	3.18	0.4337	0.0108	2.4978	0.0685	0.0416	0.0006	0.1411	0.0060	3.3326	4030	42	1271	20	263	4	2668	106
TC2101-02-13	6150	18,808	3.06	0.4370	0.0137	0.8779	0.0242	0.0146	0.0002	0.0475	0.0010	3.1639	4042	47	640	13	93	2	938	19
TC2101-02-14	1970	9912	5.03	0.1801	0.0051	0.5436	0.0168	0.0220	0.0006	0.0433	0.0017	5.3520	2654	48	441	11	140	4	857	33
TC2101-02-15	302	698	2.31	0.0529	0.0039	0.2410	0.0171	0.0332	0.0007	0.0105	0.0005	2.3725	328	168	219	14	210	4	212	10
TC2101-02-16	3478	14336	4.12	0.3525	0.0107	0.9816	0.0265	0.0203	0.0004	0.0712	0.0022	4.3614	3718	46	694	14	129	3	1390	41
TC2101-02-17	4189	12997	3.10	0.3317	0.0081	0.9490	0.0260	0.0207	0.0003	0.0488	0.0016	3.1492	3625	37	678	14	132	2	963	30
TC2101-02-18	3294	13419	4.07	0.3969	0.0189	1.0608	0.0343	0.0197	0.0004	0.0738	0.0023	4.1730	3897	72	734	17	126	3	1439	43
TC2101-02-19	367	1865	5.08	0.1499	0.0157	0.6045	0.0702	0.0289	0.0010	0.0502	0.0071	5.3191	2346	180	480	44	183	6	990	136
TC2101-02-20	354	1145	3.24	0.1147	0.0082	0.4096	0.0251	0.0265	0.0007	0.0239	0.0016	3.5663	1876	130	349	18	168	4	478	31
TC2101-02-21	461	814	1.77	0.0512	0.0042	0.2359	0.0186	0.0335	0.0007	0.0111	0.0004	1.8278	256	186	215	15	213	4	223	8
TC2101-02-22	4745	15,861	3.34	0.3043	0.0093	0.6984	0.0253	0.0166	0.0003	0.0396	0.0017	3.4729	3492	47	538	15	106	2	785	34
TC2101-02-23	5486	15,041	2.74	0.2278	0.0090	0.4441	0.0206	0.0142	0.0006	0.0207	0.0010	2.9592	3037	63	373	14	91	4	414	19
TC2101-02-24	876	1252	1.43	0.0526	0.0036	0.2267	0.0152	0.0312	0.0006	0.0098	0.0004	1.4447	322	157	207	13	198	4	197	8
TC2101-02-25	3242	9163	2.83	0.2618	0.0115	0.5051	0.0134	0.0145	0.0007	0.0243	0.0007	3.0139	3258	69	415	9	93	4	486	13
TC2101-02-26	2051	7023	3.42	0.2409	0.0143	0.9982	0.0437	0.0304	0.0008	0.0568	0.0015	3.7256	3128	94	703	22	193	5	1116	28
TC2101-02-27	1597	5556	3.48	0.1206	0.0053	0.4931	0.0202	0.0297	0.0005	0.0262	0.0010	3.6172	1965	79	407	14	188	3	522	19

Table A1. *Cont.*

Measurement Points Number	^{232}Th	^{238}U	^{232}Th/U^{238}	Isotope Ratio									Isotope Age Values (Ma)							
	ppm			^{207}Pb/^{206}Pb	±2σ	^{207}Pb/^{235}U	±2σ	^{206}Pb/^{238}U	±2σ	^{208}Pb/^{232}Th	±2σ	^{238}U/^{232}Th	^{207}Pb/^{206}Pb	±2σ	^{207}Pb/^{235}U	±2σ	^{206}Pb/^{238}U	±2σ	^{208}Pb/^{232}Th	±2σ
TC2101-02-28	1971	7213	3.66	0.1093	0.0041	0.2793	0.0100	0.0186	0.0005	0.0139	0.0004	3.6104	1788	69	250	8	119	3	278	8
TC2101-02-29	893	3209	3.59	0.0587	0.0030	0.2405	0.0121	0.0297	0.0005	0.0118	0.0004	3.5895	554	113	219	10	188	3	238	9
TC2101-02-30	3241	9483	2.93	0.2201	0.0104	0.5570	0.0171	0.0190	0.0009	0.0269	0.0008	3.0504	2981	76	450	11	121	6	536	16
ZK1798-1, granitic fine-grained rock, weighted mean of 25 points = 201.02 ± 0.42 | 0.83 | 4.37 Ma (n = 25/25) MSWD = 24.9, p(c2) = 0 (excluding points 04, 22, 28, 29)																				
ZK1798-1-01	1107	4431	4.00	0.1246	0.0213	1.2476	0.4607	0.0463	0.0070	0.0415	0.0156	3.7503	2033	307	822	208	292	43	821	303
ZK1798-1-02	869	3997	4.60	0.0550	0.0033	0.2516	0.0150	0.0330	0.0007	0.0106	0.0005	4.6800	409	133	228	12	209	4	213	10
ZK1798-1-03	1328	6626	4.99	0.0543	0.0043	0.2259	0.0181	0.0300	0.0006	0.0105	0.0007	5.0530	383	178	207	15	190	4	211	15
ZK1798-1-30	1847	8724	4.72	0.0513	0.0026	0.2080	0.0116	0.0292	0.0008	0.0099	0.0006	4.8235	254	117	192	10	185	5	199	12
ZK1798-1-04	1179	6271	5.32	0.0561	0.0028	0.2658	0.0135	0.0342	0.0006	0.0126	0.0005	5.3609	454	113	239	11	217	4	253	11
ZK1798-1-05	1406	7565	5.38	0.0518	0.0023	0.2399	0.0110	0.0334	0.0006	0.0110	0.0004	5.5545	280	102	218	9	212	4	221	9
ZK1798-1-06	1210	6181	5.11	0.0536	0.0033	0.2294	0.0134	0.0309	0.0007	0.0106	0.0006	5.1567	354	139	210	11	196	5	212	11
ZK1798-1-07	1042	5510	5.29	0.0510	0.0026	0.2309	0.0123	0.0327	0.0008	0.0105	0.0005	5.3247	239	117	211	10	207	5	211	10
ZK1798-1-08	1176	5256	4.47	0.0549	0.0071	0.2212	0.0240	0.0294	0.0007	0.0106	0.0008	4.6118	409	294	203	20	187	4	213	16
ZK1798-1-09	877	3864	4.41	0.0515	0.0029	0.2403	0.0142	0.0336	0.0007	0.0112	0.0005	4.5410	261	126	219	12	213	4	226	11
ZK1798-1-10	1659	8000	4.82	0.0522	0.0021	0.2041	0.0094	0.0282	0.0008	0.0094	0.0004	4.8801	295	88	189	8	179	5	188	7
ZK1798-1-11	1680	7919	4.71	0.0553	0.0034	0.2268	0.0131	0.0296	0.0006	0.0107	0.0007	4.7690	433	144	208	11	188	4	216	13
ZK1798-1-12	1121	5239	4.68	0.0546	0.0027	0.2464	0.0121	0.0326	0.0007	0.0110	0.0005	4.7342	394	113	224	10	207	4	220	11
ZK1798-1-13	1372	6340	4.62	0.0550	0.0029	0.2444	0.0140	0.0320	0.0007	0.0115	0.0008	4.7225	409	119	222	11	203	4	231	16
ZK1798-1-14	1454	6373	4.38	0.0528	0.0021	0.2405	0.0105	0.0328	0.0006	0.0110	0.0005	4.4738	320	91	219	9	208	4	221	10
ZK1798-1-15	1014	4328	4.27	0.0540	0.0036	0.2424	0.0165	0.0323	0.0006	0.0115	0.0009	4.3740	372	150	220	13	205	4	231	18
ZK1798-1-16	1443	6852	4.75	0.0505	0.0024	0.2242	0.0108	0.0321	0.0006	0.0104	0.0005	4.7952	217	109	205	9	203	4	210	10
ZK1798-1-17	1047	4560	4.36	0.0534	0.0033	0.2339	0.0139	0.0317	0.0006	0.0106	0.0006	4.4180	346	134	213	11	201	4	214	11
ZK1798-1-18	1305	5813	4.45	0.0534	0.0035	0.2356	0.0170	0.0317	0.0006	0.0112	0.0009	4.5966	346	146	215	14	201	4	225	18
ZK1798-1-19	1317	5885	4.47	0.0664	0.0039	0.2730	0.0158	0.0298	0.0005	0.0145	0.0009	4.5302	820	119	245	13	189	3	291	19
ZK1798-1-20	1730	7110	4.11	0.0546	0.0026	0.2021	0.0121	0.0268	0.0011	0.0089	0.0006	4.2066	394	107	187	10	170	7	179	11
ZK1798-1-21	865	4345	5.02	0.0520	0.0025	0.2444	0.0123	0.0340	0.0007	0.0106	0.0005	5.0889	287	111	222	10	215	4	214	10
ZK1798-1-22	3104	11,752	3.79	0.0715	0.0062	0.2646	0.0436	0.0254	0.0018	0.0114	0.0014	3.8850	972	180	238	35	162	11	229	29
ZK1798-1-23	949	4771	5.03	0.0520	0.0027	0.2429	0.0141	0.0336	0.0007	0.0115	0.0007	5.0935	283	150	221	12	213	4	231	14
ZK1798-1-24	1355	6506	4.80	0.0500	0.0026	0.2210	0.0115	0.0319	0.0007	0.0104	0.0005	4.8728	195	116	203	10	203	4	209	11
ZK1798-1-25	1365	6146	4.50	0.0563	0.0030	0.2419	0.0137	0.0310	0.0007	0.0120	0.0007	4.5848	465	123	220	11	197	5	242	14
ZK1798-1-26	1476	7234	4.90	0.0523	0.0031	0.2200	0.0133	0.0303	0.0006	0.0102	0.0004	5.0472	298	131	202	11	193	4	206	9
ZK1798-1-27	1615	7084	4.39	0.0554	0.0051	0.2381	0.0207	0.0312	0.0007	0.0116	0.0013	4.4490	428	206	217	17	198	4	232	26
ZK1798-1-28	1398	6194	4.43	0.0639	0.0036	0.2795	0.0174	0.0314	0.0007	0.0148	0.0009	4.4834	739	119	250	14	199	4	296	18
ZK1798-1-29	1525	6744	4.42	0.0585	0.0042	0.2398	0.0170	0.0295	0.0006	0.0113	0.0008	4.5276	550	157	218	14	188	4	227	15

Table A2. Major (wt%) and trace (ppm) elemental test data of granitic dykes in the Yangshan gold belt.

Sample Number	311-8-2	311-8-4	311-8-5	311-8-8	21ZJS03	21ZJS04	21ZJS05	21ZJS06	ZK1798-2	ZK1798-3	ZK1798-4	21NS02	21NS03	21NS04	21PZb-02	21PZb-03	21SCKy02	21SCKy03	21SCKy04	21BS02	21BS03	21XG02	21XG03	TC2101-03	TC2101-04
SiO_2%	75.11	74.89	74.47	74.72	75.67	73.88	73.18	75.94	84.17	84.53	84.12	74.56	75.12	73.34	71.99	72.42	76.08	76.72	76.71	78.25	81.52	72.59	74.43	76.55	76.28
TiO_2%	0.26	0.28	0.29	0.29	0.34	0.37	0.38	0.37	0.07	0.06	0.06	0.22	0.22	0.23	0.36	0.37	0.03	0.03	0.03	0.02	0.02	0.26	0.26	0.23	0.22
Al_2O_3%	16.41	16.82	17.13	16.79	16.28	16.93	17.29	15.83	10.40	10.09	10.41	15.04	15.21	16.01	15.66	16.06	14.03	13.31	13.58	14.96	10.64	15.82	14.70	14.93	15.09
Fe_2O_3-T%	1.86	1.88	2.09	2.10	2.29	2.44	2.46	2.10	0.72	0.70	0.72	1.43	1.60	1.48	2.37	2.27	0.43	0.48	0.47	0.56	0.48	1.87	1.80	1.48	1.95
MnO%	0.03	0.03	0.03	0.03	0.04	0.04	0.04	0.04	0.02	0.02	0.02	0.02	0.02	0.03	0.04	0.03	0.03	0.03	0.03	0.05	0.04	0.03	0.03	0.03	0.05
MgO%	0.77	0.65	0.72	0.67	0.28	0.31	0.33	0.27	0.16	0.16	0.17	0.43	0.45	0.45	0.79	0.64	0.09	0.08	0.09	0.13	0.03	0.48	0.29	0.22	0.24
CaO%	1.26	0.90	1.28	1.06	1.55	1.86	2.00	1.27	0.43	0.43	0.46	1.25	0.79	1.25	1.80	1.32	0.91	1.14	1.02	2.34	1.04	2.35	2.13	1.93	2.66
Na_2O%	0.13	0.12	0.08	0.10	0.09	0.10	0.11	0.14	0.87	0.72	0.75	4.54	3.39	4.59	3.08	2.73	4.35	4.27	4.22	0.10	4.01	3.29	3.68	0.27	0.42
K_2O%	3.47	3.51	3.09	3.36	3.07	3.56	3.71	3.89	2.80	2.96	2.96	2.14	2.78	2.21	3.37	3.65	3.52	3.63	3.51	3.16	2.12	2.96	2.29	3.75	2.82
P_2O_5%	0.09	0.09	0.09	0.09	0.10	0.12	0.11	0.09	0.03	0.04	0.04	0.08	0.08	0.08	0.11	0.11	0.02	0.03	0.02	0.01	0.01	0.08	0.08	0.07	0.07
LOI%	4.43	4.20	5.02	4.57	4.62	4.79	5.00	3.81	2.83	2.65	2.65	2.88	2.65	2.70	3.48	3.12	1.51	1.75	1.67	4.20	2.11	3.96	3.72	4.32	4.95
Total	99.40	99.16	99.28	99.22	99.70	99.61	99.61	99.93	99.68	99.70	99.72	99.72	99.66	99.68	99.58	99.61	99.50	99.73	99.69	99.59	99.91	99.73	99.68	99.46	99.80
NK	3.60	3.63	3.18	3.46	3.16	3.66	3.82	4.02	3.67	3.68	3.71	6.68	6.17	6.80	6.44	6.39	7.87	7.90	7.73	3.26	6.14	6.25	5.96	4.02	3.24
CNK	4.86	4.52	4.46	4.52	4.70	5.52	5.82	5.29	4.10	4.11	4.17	7.93	6.96	8.05	8.25	7.70	8.78	9.04	8.75	5.60	7.17	8.60	8.09	5.95	5.90
A/CNK	3.38	3.72	3.84	3.71	3.46	3.06	2.97	2.99	2.53	2.45	2.49	1.90	2.19	1.99	1.90	2.08	1.60	1.47	1.55	2.67	1.48	1.84	1.82	2.51	2.56
A/NK	4.56	4.64	5.39	4.85	5.15	4.63	4.53	3.93	2.83	2.74	2.81	2.25	2.46	2.35	2.43	2.51	1.78	1.68	1.76	4.59	1.73	2.53	2.46	3.72	4.66
Li	41.00	66.90	86.00	41.10	43.50	40.00	42.00	33.10	38.00	26.80	27.80	13.70	10.30	12.30	47.00	62.20	47.90	48.30	49.70	19.30	13.30	47.60	214.00	115.00	78.20
Be	3.00	3.35	3.40	2.96	2.80	3.17	3.22	3.28	3.16	3.16	3.18	4.04	4.17	4.15	3.15	3.42	4.51	4.91	5.14	5.39	4.51	3.50	3.36	4.22	4.68
Sc	4.06	3.29	3.50	3.54	3.20	1.00	3.88	3.06	2.24	2.49	2.46	5.51	4.74	5.65	5.89	5.88	4.62	4.60	4.45	2.54	4.48	6.15	5.34	3.17	2.35
V	17.00	19.20	18.90	18.60	23.30	25.30	25.20	24.90	0.96	0.75	0.79	13.00	13.40	14.20	25.60	25.60	0.31	0.31	0.26	0.30	0.32	18.30	17.60	14.20	12.90
Cr	7.07	9.12	9.48	9.62	4.45	6.60	4.53	5.58	3.29	2.57	0.74	10.20	9.93	10.50	5.12	10.70	1.26	6.95	1.79	2.55	5.69	13.00	12.80	7.27	8.78
Co	3.65	4.27	4.10	4.08	3.14	3.62	3.58	3.16	0.37	0.37	0.34	1.50	2.87	1.74	4.08	3.42	0.37	0.42	0.34	0.34	0.33	2.45	3.46	2.43	2.10
Ni	2.16	3.00	2.80	2.43	2.37	3.18	3.65	2.72	0.64	nd	nd	4.59	6.33	4.62	3.14	4.11	1.37	5.35	1.05	1.60	2.18	4.31	4.46	3.72	4.35
Cu	6.79	13.90	14.60	10.80	9.79	12.90	13.00	6.09	4.61	5.33	4.40	10.60	14.50	11.70	11.00	17.00	0.50	0.95	0.78	0.81	1.09	12.10	12.90	5.94	5.73
Zn	46.40	46.10	47.80	52.30	53.40	53.80	55.80	45.70	41.00	37.10	42.40	32.00	43.00	34.00	60.80	61.50	42.70	48.20	45.20	24.70	21.90	41.00	45.60	52.80	52.50
Ga	20.60	20.80	20.70	20.80	20.10	21.80	22.20	21.70	18.00	18.30	18.40	20.60	21.00	21.40	20.80	22.20	22.30	21.70	23.00	23.70	21.40	20.00	19.80	22.80	22.00
As	2490.0	4430.0	3430.0	4370.0	19.70	21.50	19.70	34.70	3.36	2.53	1.85	5.30	15.30	4.18	6.36	7.12	7.12	8.11	2.75	16.50	74.40	22.70	26.00	82.10	7.51
Rb	182.00	180.00	146.00	170.00	137.00	156.00	161.00	168.00	127.00	141.00	142.00	107.00	123.00	114.00	123.00	138.00	201.00	206.00	201.00	185.00	110.00	131.00	102.00	196.00	162.00
Sr	96.40	94.00	134.00	79.40	124.00	184.00	217.00	206.00	89.20	76.50	77.60	209.00	119.00	233.00	213.00	125.00	64.10	85.30	85.80	181.00	76.20	210.00	210.00	56.70	79.30
Y	7.75	7.14	8.02	7.89	8.18	8.65	9.04	8.01	6.63	7.03	7.20	8.10	8.00	8.48	9.18	9.80	11.40	11.50	11.60	13.70	10.40	7.88	8.13	10.60	11.40
Zr	91.90	99.80	97.60	99.10	109.00	127.00	119.00	118.00	49.90	48.60	50.00	93.00	97.00	97.50	131.00	124.00	32.60	31.40	35.10	26.80	27.30	103.00	107.00	76.90	73.10
Nb	6.75	7.18	7.39	7.46	6.58	9.51	7.71	7.27	9.26	9.15	9.15	8.62	8.72	8.85	7.15	8.47	11.30	10.70	11.10	13.90	12.80	7.20	7.38	10.00	9.39
Cs	21.50	27.30	19.40	25.40	9.98	10.10	9.80	10.10	8.75	8.17	8.32	8.87	9.82	8.40	7.13	7.25	10.80	10.70	10.70	19.30	6.86	14.30	14.30	14.30	21.40
Ba	514.00	563.00	495.00	496.00	348.00	424.00	441.00	569.00	430.00	401.00	405.00	276.00	264.00	293.00	675.00	941.00	427.00	480.00	521.00	91.30	43.10	231.00	474.00	297.00	244.00
La	19.00	20.90	19.80	21.90	20.30	21.10	21.90	19.40	14.10	11.90	11.10	21.30	21.30	21.50	19.60	22.90	7.59	7.49	9.14	2.36	1.97	19.50	19.80	10.00	10.60
Ce	30.40	34.00	32.10	38.80	32.70	33.80	35.10	31.00	23.40	20.00	18.60	34.80	34.20	35.20	32.00	39.60	13.50	13.30	16.20	4.29	3.34	32.30	32.20	16.80	17.70
Pr	3.85	4.38	4.07	4.50	4.18	4.29	4.51	3.91	3.08	2.62	2.41	4.46	4.46	4.45	4.09	4.81	1.82	1.79	2.17	0.66	0.54	4.12	4.19	2.21	2.38
Nd	13.60	15.90	14.70	16.10	15.10	15.70	16.60	13.90	11.40	9.81	9.20	16.00	16.10	15.90	14.90	17.60	6.79	6.81	8.08	2.97	2.46	14.90	15.10	8.56	9.28
Sm	2.80	3.38	3.22	3.31	2.97	3.11	3.23	2.75	2.94	2.71	2.61	3.36	3.47	3.38	2.94	3.49	2.31	2.40	2.49	1.70	1.34	3.11	3.20	2.25	2.57
Eu	0.69	0.77	0.87	0.78	0.72	0.77	0.78	0.71	0.65	0.53	0.53	0.71	0.73	0.73	0.76	0.75	0.36	0.38	0.37	0.31	0.25	0.72	0.71	0.49	0.67
Gd	2.43	2.57	2.90	2.66	2.47	2.63	2.69	2.32	2.58	2.54	2.45	2.92	2.94	2.96	2.48	2.95	2.48	2.53	2.49	2.35	1.89	2.61	2.66	2.31	2.68
Tb	0.34	0.33	0.39	0.35	0.34	0.35	0.37	0.33	0.35	0.36	0.35	0.40	0.41	0.40	0.35	0.40	0.42	0.43	0.42	0.43	0.34	0.36	0.36	0.37	0.41
Dy	1.55	1.46	1.69	1.58	1.63	1.68	1.76	1.56	1.57	1.66	1.65	1.75	1.78	1.87	1.73	1.92	2.23	2.27	2.24	2.50	1.98	1.62	1.67	2.02	2.19
Ho	0.25	0.24	0.26	0.26	0.28	0.29	0.30	0.27	0.23	0.23	0.24	0.26	0.26	0.27	0.33	0.32	0.35	0.36	0.35	0.41	0.33	0.26	0.26	0.33	0.36
Er	0.70	0.67	0.71	0.72	0.79	0.83	0.87	0.77	0.57	0.59	0.59	0.67	0.67	0.70	0.87	0.92	0.89	0.90	0.91	1.05	0.83	0.70	0.72	0.90	0.95
Tm	0.09	0.09	0.09	0.10	0.11	0.11	0.12	0.11	0.07	0.07	0.07	0.08	0.08	0.09	0.12	0.13	0.12	0.12	0.13	0.15	0.12	0.09	0.10	0.12	0.14
Yb	0.57	0.56	0.58	0.60	0.69	0.71	0.74	0.68	0.41	0.42	0.43	0.49	0.52	0.52	0.77	0.79	0.74	0.73	0.76	0.88	0.69	0.58	0.60	0.76	0.81
Lu	0.08	0.08	0.08	0.08	0.10	0.10	0.11	0.10	0.06	0.06	0.06	0.07	0.07	0.07	0.11	0.11	0.10	0.10	0.10	0.12	0.09	0.08	0.09	0.11	0.11
Hf	2.52	2.63	2.67	2.72	3.09	3.39	3.34	3.26	1.99	1.96	2.00	2.78	2.89	2.93	3.70	3.63	1.86	1.75	1.95	1.95	1.98	2.98	3.12	2.73	2.35
Ta	0.76	0.78	0.87	0.86	0.66	0.90	0.73	0.68	1.23	1.13	1.10	1.18	1.18	1.24	0.72	1.20	2.01	1.96	2.09	1.84	1.86	0.83	0.89	1.23	1.08
Tl	0.83	0.84	0.68	0.80	0.61	0.68	0.74	0.79	0.64	0.67	0.67	0.48	0.62	0.52	0.59	0.65	0.95	0.97	0.92	0.94	0.61	0.77	0.83	0.94	0.73
Pb	13.60	21.60	20.50	23.10	19.00	15.90	12.50	8.69	34.50	30.90	27.70	21.50	26.20	20.40	24.80	24.20	25.70	30.80	29.70	13.50	22.50	22.20	20.90	34.30	38.50
Th	7.72	7.59	7.46	8.25	7.31	6.75	7.79	6.92	6.94	6.32	6.45	8.17	8.19	8.76	7.80	8.54	7.77	7.91	9.19	4.31	3.82	7.83	8.18	6.79	6.45
U	3.89	3.90	4.03	4.16	2.79	2.16	2.83	2.79	4.53	5.35	6.19	4.44	4.19	4.65	3.47	3.66	10.90	15.50	7.59	2.63	2.70	2.78	2.85	3.40	2.73
ΣREE	76.34	85.32	81.47	91.74	82.36	85.47	89.06	77.80	61.41	53.49	50.29	87.27	86.99	88.04	81.04	96.69	39.71	39.60	45.86	20.17	16.17	80.94	81.66	47.22	50.85
LREE	70.34	79.33	74.76	85.39	75.97	78.77	82.12	71.67	55.57	47.57	44.45	80.63	80.26	81.16	74.29	89.15	32.37	32.17	38.45	12.29	9.90	74.65	75.20	40.31	43.20
HREE	6.00	5.99	6.71	6.35	6.40	6.70	6.94	6.13	5.84	5.92	5.84	6.64	6.73	6.89	6.75	7.54	7.34	7.44	7.40	7.88	6.27	6.29	6.46	6.91	7.65
LREE/HREE	11.73	13.25	11.15	13.45	11.87	11.76	11.83	11.69	9.52	8.03	7.61	12.14	11.92	11.79	11.00	11.82	4.41	4.33	5.20	1.56	1.58	11.87	11.65	5.83	5.65
La_N/Yb_N	23.99	27.01	24.40	26.18	21.07	21.41	21.26	20.59	24.55	20.37	18.69	30.93	29.55	29.43	18.21	20.82	7.34	7.34	8.58	1.92	2.04	24.16	23.83	9.49	9.34
δEu	0.79	0.77	0.85	0.78	0.79	0.80	0.78	0.84	0.71	0.61	0.63	0.67	0.68	0.69	0.84	0.70	0.45	0.46	0.45	0.47	0.49	0.75	0.72	0.65	0.77
δCe	0.82	0.83	0.83	0.91	0.82	0.82	0.82	0.82	0.83	0.84	0.84	0.83	0.82	0.84	0.83	0.88	0.86	0.86	0.86	0.83	0.78	0.84	0.82	0.84	0.83

Table A3. Zircon Hf isotope analytical data of granitic dyke samples from the Yangshan gold belt.

Sample No.	t (Ma)	^{176}Hf/^{177} Hf	1σ	^{176}Lu/^{177} Hf	1σ	^{176}Yb/^{177} Hf	1σ	εHf (0)	1σ	εHf (t)	1σ	$T_{DM}{}^{1}$ (Ma)	$T_{DM}{}^{2}$ (Ma)	$f_{Lu/Hf}$
Granitic dyke 21PZB-01														
21PZB-01-02	213.306	0.282602	0.000017	0.001286	0.000003	0.035072	0.000115	−6.0	0.8	−1.5	0.8	927	1201	−0.96
21PZB-01-03	213.559	0.282605	0.000016	0.000975	0.000004	0.024987	0.000078	−5.9	0.8	−1.4	0.8	916	1194	−0.97
21PZB-01-04	213.798	0.282612	0.000017	0.001147	0.000010	0.032381	0.000246	−5.7	0.8	−1.1	0.8	910	1181	−0.97
21PZB-01-06	212.235	0.282604	0.000017	0.000917	0.000021	0.024753	0.000541	−5.9	0.8	−1.4	0.8	915	1195	−0.97
21PZB-01-07	210.487	0.282613	0.000017	0.001514	0.000020	0.039953	0.000478	−5.6	0.8	−1.2	0.8	917	1183	−0.95
21PZB-01-10	211.765	0.282633	0.000023	0.000961	0.000010	0.026325	0.000283	−4.9	1.0	−0.4	1.0	876	1139	−0.97
21PZB-01-11	214.313	0.282619	0.000017	0.000991	0.000012	0.026652	0.000447	−5.4	0.8	−0.8	0.8	895	1164	−0.97
21PZB-01-15	214.680	0.282593	0.000021	0.001151	0.000007	0.031677	0.000292	−6.3	0.9	−1.8	0.9	937	1218	−0.97
21PZB-01-16	212.015	0.282623	0.000018	0.001636	0.000008	0.043933	0.000224	−5.3	0.8	−0.9	0.8	906	1164	−0.95
21PZB-01-20	213.852	0.282649	0.000021	0.001610	0.000006	0.050533	0.000209	−4.4	0.9	0.1	0.9	868	1111	−0.95
21PZB-01-22	212.794	0.282618	0.000020	0.001655	0.000009	0.047432	0.000189	−5.4	0.9	−1.0	0.9	913	1172	−0.95
Granitic dyke 21ZJS-01														
21ZJS-01-02	214.626	0.282625	0.000016	0.000736	0.000006	0.019765	0.000243	−5.2	0.8	−0.6	0.8	881	1151	−0.98
21ZJS-01-03	209.379	0.282627	0.000018	0.001313	0.000012	0.036492	0.000408	−5.1	0.8	−0.7	0.8	892	1154	−0.96
21ZJS-01-04	206.247	0.282634	0.000014	0.000286	0.000004	0.008983	0.000180	−4.9	0.7	−0.4	0.7	859	1134	−0.99
21ZJS-01-17	211.446	0.282630	0.000018	0.001150	0.000034	0.031073	0.000988	−5.0	0.8	−0.5	0.8	884	1146	−0.97
21ZJS-01-18	208.067	0.282626	0.000018	0.001072	0.000009	0.029765	0.000269	−5.2	0.8	−0.8	0.8	888	1155	−0.97

[1] Footnotes: $\varepsilon Hf(0) = ((^{176}Hf/^{177}Hf)_s/(^{176}Hf/^{177}Hf)_{CHUR,0} - 1) \times 10{,}000$; $\varepsilon Hf(t) = (((^{176}Hf/^{177}Hf)_s - (^{176}Lu/^{177}Hf)_s \times (e^{\lambda t} - 1))/((^{176}Hf/^{177}Hf)_{CHUR,0} - (^{176}Lu/^{177}Hf)_{CHUR} \times (e^{\lambda t} - 1)) - 1) \times 10{,}000$; $T_{DM}{}^{1} = 1/\lambda \times \ln [1 + ((^{176}Hf/^{177}Hf)_s - (^{176}Hf/^{177}Hf)_{DM})/((^{176}Lu/^{177}Hf)_s - (^{176}Lu/^{177}Hf)_{DM})]$. $T_{DM}{}^{2} = T_{DM}{}^{1} - (T_{DM}{}^{1} - t)((f_{cc} - f_s)/(f_{cc} - f_{DM}))$. $f_{Lu/Hf} = (^{176}Lu/^{177}Hf)_s/(^{176}Lu/^{177}Hf)_{CHUR} - 1$.

References

1. Dong, Y.-P.; Zhang, G.-W.; Neubauer, E.; Liu, X.-M.; Genser, J.; Hauzenberger, C. Tectonic evolution of the Qinling orogen, China: Review and synthesis. *J. Asian Earth Sci.* **2011**, *41*, 213–237. [CrossRef]
2. Dong, Y.-P.; Santosh, M. Tectonic architecture and multiple orogeny of the Qinling Orogenic Belt, Central China. *Gondwana Res.* **2016**, *29*, 1–40. [CrossRef]
3. Han, D. *Specification of Geological Map I48E018011 1:50,000 in the Area of Buziba*; Gansu Geological Survey Bureau No. 3; Geological Survey Institute: Lanzhou, China, 1999.
4. Qi, J.-Z.; Yuan, S.-S.; Liu, Z.-J.; Liu, D.-Y.; Wang, Y.-B.; Li, Z.-H.; Guo, J.-H.; Sun, B. U-Pb SHRIMP Dating of Zircon from Quartz Veins of the Yangshan Gold Deposit in Gansu Province and Its Geological Significance. *Acta Geol. Sin.* **2004**, *78*, 443–451.
5. Qi, J.-Z.; Li, L.; Yuan, S.-S.; Liu, Z.-J.; Liu, D.-Y.; Wang, Y.-B.; Li, Z.-H. A Shrimp U–Pb chro-nological study of zircons from quartz veins of Yangshan gold deposit, Gansu Province. *Miner. Depos.* **2005**, *24*, 141–150, (In Chinese with English abstract).
6. Qi, J.-Z.; Yang, G.-C.; Li, L.; Fan, Y.-X.; Liu, W. Isotope geochemistry, chronology and genesis of the Yangshan gold deposit Gansu. *Geol. China* **2006**, *33*, 1345–1353, (In Chinese with English abstract).
7. Yan, F.-Z.; Li, Q.-Z. Yangshan Gold Deposit: The Largest Carlin and Carlin-like Type Gold Deposit in China. *Acta Geol. Sin.* **2008**, *82*, 804–810.
8. Lei, S.-B. Tectonic and Magmatic Constraints on Mineralization and Gold Prospecting of Yangshan Gold Belt, Gansu Province. Ph.D. Thesis, China University of Geosciences, Beijing, China, 2011. (In Chinese with English abstract).
9. Yang, L.-Q.; Ji, X.-Z.; Santosh, M.; Li, N.; Zhang, Z.-C.; Yu, J.-Y. Detrital zircon u–pb ages, hf isotope, and geochemistry of devonian chert from the mianlue suture: Implications for tectonic evolution of the Qinling orogen. *J. Asian Earth Sci.* **2015**, *113*, 589–609. [CrossRef]
10. Yang, G.-C.; Yuan, S.-S.; Ge, L.-S.; Wang, Z.-H.; Qi, J.-Z.; Yan, J.-P.; Zhao, Y.-Z.; Zhang, Y.-J.; Li, P. Petrogenesis of Granites in Yangshan Gold Deposit, Gansu Province: Evidence from Geochemical Characteristics, Sr-Nd-Pb Isotope and Geochronology. *Geotecton. Metallog.* **2016**, *40*, 739–752, (In Chinese with English abstract).
11. Guo, Y.-Y. Indochinese Orogenic Gold Mineralization Deposits in the Southern Belt of the West Qinling, Central China. Ph.D. Thesis, China University of Geosciences, Beijing, China, 2016. (In Chinese with English abstract).
12. Yang, L.-Q.; Deng, J.; Li, N.; Zhangn, C.; Ji, X.-Z.; Yu, J.-Y. Isotopic characteristics of gold deposits in the Yangshan Gold Belt, West Qinling, central China: Implications for fluid and metal sources and ore genesis. *J. Geochem. Explor.* **2016**, *168*, 103–118. [CrossRef]
13. Liang, J.-L.; Sun, W.-D.; Li, Y.-L.; Zhu, S.-Y.; Li, H.; Liu, Y.-L.; Zhai, W. An xps study on the valence states of arsenic in arsenian pyrite: Implications for au deposition mechanism of the yang-shan carlin-type gold deposit, western qinling belt. *J. Asian Earth Sci.* **2013**, *62*, 363–372. [CrossRef]
14. Liang, J.-L.; Sun, W.-D.; Zhu, S.-Y.; Li, H.; Liu, Y.-L.; Zhai, W. Mineralogical study of sediment-hosted gold deposits in the Yangshan ore field, Western Qinling Orogen, Central China. *J. Asian Earth Sci.* **2014**, *85*, 40–50. [CrossRef]
15. Liang, J.-L.; Li, J.; Sun, W.-D.; Zhao, J.; Zhai, W.; Huang, Y.; Song, M.-C.; Ni, S.J.; Xiang, Q.R.; Zhang, J.C.; et al. Source of ore-forming fluids of the Yangshan gold field, western Qinling orogen, China: Evidence from microthermometry, noble gas isotopes and in situ sulfur isotopes of Au-carrying pyrite. *Ore Geol. Rev.* **2019**, *105*, 404–422. [CrossRef]
16. Li, N.; Deng, J.; Yang, L.-Q.; Groves, D.L.; Liu, X.-W.; Dai, W.-G. Constraints on depositional conditions and ore-fluid source for orogenic gold districts in the West Qinling Orogen, China: Implications from sulfide assemblages and their trace-element geochemistry. *Ore Geol. Rev.* **2018**, *102*, 204–219. [CrossRef]
17. Yang, R.S. Geological Geochemistry Characteristics and Genesis of the Yangshan Gold Deposit, Gansu Province, China. Ph.D. Thesis, Peking University, Beijing, China, 2006. (In Chinese with English abstract).
18. Yang, L.-Q.; Deng, J.; Dilek, Y.; Qiu, K.-F.; Ji, X.-Z.; Li, N.; Taylor, R.-D.; Yu, J.-Y. Structure, geochronology, and petrogenesis of the late triassic puziba granitoid dikes in the mianlue suture zone, Qinling orogen, China. *Geol. Soc. Am. Bull.* **2015**, *127*, 1–25. [CrossRef]
19. Yang, Z.-H.; Xiong, T.; Gou, Z.-Y.; Li, H.; Wang, L. LA-ICP-MS fission track thermochronology of apatite in the Yangshan gold ore belt, southern margin of West Qinling. *Acta Geol. Sin.* **2022**, *96*, 3849–3866, (In Chinese with English abstract).
20. Sun, S.H. Geological and geochemical signature of Carlin-like gold deposit in the north Sichuan-South Gansu area. *Collect. Geol. Explor.* **2005**, *20*, 8–14, (In Chinese with English abstract).
21. Wang, Z.-H. Coupling Relationship between Large-Scale Mineralization and Major Geological Event in the Yangshan Gold Ore Belt, Gansu Province. Ph.D. Thesis, China University of Geosciences, Beijing, China, 2018. (In Chinese with English abstract).
22. Guo, Y.-P. Magmatism and Resource Prospects of Getiaowan Mine Section of Yangshan Gold Belt, Wenxian, Gansu. Master's Thesis, Chengdu University of Technology, Chengdu, China, 2020. (In Chinese with English abstract).
23. Li, J.; Chen, Y.-J.; Li, Q.-Z.; Lai, Y.; Yang, R.-S.; Mao, S.-D. Fluid inclusion geochemistry and genetic type of the Yangshan gold deposit, Gansu, China. *Acta Petrol. Sin.* **2007**, *23*, 2144–2154, (In Chinese with English abstract).
24. Li, N.; Zhang, Z.-C.; Liu, X.-W.; Liu, J. The relationship between disseminated gold mineralization and vein-type gold-antimony mineralization: Example from the Yangshan gold belt, West Qinling. *Acta Petrol. Sin.* **2018**, *34*, 1312–1326, (In Chinese with English abstract).
25. Liu, Y.-S.; Hu, Z.-C.; Gao, S.; Günther, D.; Xu, J.; Gao, C.-G.; Chen, H.-H. In situ analysis of major and trace elements of anhydrous minerals by LA-ICP-MS without applying an internal standard. *Chem. Geol.* **2008**, *257*, 34–43. [CrossRef]

26. Liu, Y.-S.; Gao, S.; Hu, Z.-C.; Gao, C.-G.; Zong, K.-Q.; Wang, D.-B. Continental and oceanic crust recycling-induced melt-peridotite interactions in the Trans-North China Orogen: U-Pb dating, Hf isotopes and trace elements in zircons of mantle xenoliths. *J. Petrol.* **2010**, *51*, 537–571. [CrossRef]
27. Potts, P.-J.; Kane, J.-S. International Association of Geoanalysts Certificate of Analysis: Certified Reference Material OU-6 (Penrhyn Slate). *Geostand. Geoanal. Res.* **2010**, *29*, 233–236. [CrossRef]
28. Hu, Z.-C.; Liu, Y.-S.; Gao, S.; Xiao, S.-Q.; Zhao, L.-S.; Günther, D.; Li, M.; Zhang, W.-Z.; Zong, K.-Q. A "wire" signal smoothing device for laser ablation inductively coupled plasma mass spectrometry analysis. *Spectrochim. Acta Part B Atom. Spectrosc.* **2012**, *78*, 50–57. [CrossRef]
29. Hu, Z.-C.; Liu, Y.-S.; Gao, S.; Liu, W.-G.; Zhang, W.; Tong, X.-R.; Lin, L.; Zong, K.-Q.; Li, M.; Chen, H.-H.; et al. Improved in situ Hf isotope ratio analysis of zircon using newly designed X skimmer cone and Jet sample cone in combination with the addition of nitrogen by laser ablation multiple collector ICP-MS. *J. Anal. Atom. Spectrom.* **2012**, *27*, 1391–1399. [CrossRef]
30. Scherer, E.; Munker, C.; Mezger, K. Calibration of the lutetium-hafnium clock. *Science* **2001**, *293*, 683–687. [CrossRef]
31. Albarède, F.; Blichert-Toft, J. The Lu-Hf isotope geochemistry of chondrites and the evolution of the mantle-crust system. *Earth Planet. Sci. Lett.* **1997**, *148*, 243–258.
32. Vervoort, J.-D.; Blichert-Toft, J. Evolution of the depleted mantle: Hf isotope evidence from juvenile rock through time. *Geochim. Cosmochim. Acta* **1999**, *63*, 533–556. [CrossRef]
33. Hoskin, P.; Schaltegger, U. The Composition of Zircon and Igneous and Metamorphic Petrogenesis. *Rev. Mineral. Geochem.* **2003**, *53*, 27–62. [CrossRef]
34. Middlemost, E. Naming materials in the magma/igneous rock system. *Earth-Sci. Rev.* **1994**, *37*, 215–224. [CrossRef]
35. Rollinson, H. *Using Geochemical Data: Evaluation, Presentation, Interpretation*; Longman Scientific and Technical: New York, NY, USA, 1993; pp. 1–352.
36. Maniar, P.D.; Piccoli, P.M. Tectonic discrimination of granitoids. *GSA Bull.* **1989**, *101*, 635–643. [CrossRef]
37. Sun, S.-S.; McDonough, W.F. Chemical and isotopic systematics of oceanic basalts: Implications for mantle composition and processes. *Geol. Soc. Lond. Spec. Publ.* **1989**, *42*, 313–345. [CrossRef]
38. Taylor, S.R.; Mclennan, S.M. *The Continental Crust: Its Composition and Evolution*; An Examination of the Geochemical Record Preserved in Sedimentary Rock; Blackwell Scientific Publication: Hoboken, NJ, USA, 1985; pp. 1–328.
39. Liu, H.-J.; Mao, S.-D.; Zhao, C.-H.; Yang, R.-S. Element and Sr-Nb-Pb isotope geochemistry of ganite-porphyry dykes in the Yangshan gold belt, western Qinling Orogen. *Acta Petrol. Sin.* **2008**, *24*, 1101–1111, (In Chinese with English abstract).
40. Ferry, J.M.; Watson, E.B. New thermodynamic models and revised calibrations for the Ti-in-zircon and Zr-in-rutile thermometers. *Contrib. Mineral. Petrol.* **2007**, *154*, 429–437. [CrossRef]
41. Whalen, J.B.; Currie, K.L.; Chappell, B.W. A-type granites: Geochemical characteristics, discrimination and petrogenesis. *Contrib. Mineral. Petrol.* **1987**, *95*, 407–419. [CrossRef]
42. Collins, W.J.; Beams, S.D.; White, A.J.R.; Chappell, B.W. Nature and origin of A-type granites with particular reference to southeastern Australia. *Contrib. Mineral. Petrol.* **1982**, *80*, 189–200. [CrossRef]
43. Chappell, B.W. Aluminium saturation in I- and S-type granites and the characterization of fractionated haplogranites. *Lithosphere* **1999**, *46*, 535–551. [CrossRef]
44. Wu, F.-Y.; Jahn, B.-M.; Wilde, S.A.; Lo, C.-H.; Yui, T.-F.; Lin, Q.; Ge, W.-C.; Sun, D.-Y. Highly fractionated I-type granites in NE China (II): Isotopic geochemistry and implications for crustal growth in the Phanerozoic. *Lithosphere* **2003**, *67*, 191–204. [CrossRef]
45. Li, X.-H.; Li, Z.-X.; Li, W.-X.; Ying, L.; Yuan, C.; Wei, G.; Qi, C. U–Pb zircon, geochemical and Sr–Nd–Hf isotopic constraints on age and origin of Jurassic I- and A-type granites from central Guangdong, China: A major igneous event in response to foundering of a subducted flat-slab? *Lithosphere* **2007**, *96*, 186–204. [CrossRef]
46. Yan, Q.-R.; Wang, Z.-Q.; Hanson, A.D.; Druschke, P.A.; Zhen, Y.; Liu, D.-Y.; Jian, P.; Song, B.; Wang, T.; Jiang, C.F. Shrimp Age and Geochemistry of the Bikou Volcanic Terrane: Implications for Neoproterozoic Tectonics on the Northern Margin of the Yangtze Craton. *Acta Geol. Sin. (Engl. Ed.)* **2003**, *77*, 479–490.
47. Yan, Q.-R.; Hanson, A.; Wang, Z.-Q.; Druschke, P.; Yan, Z.; Wang, T.; Liu, D.-Y.; Song, B.; Jian, P.; Zhou, H.; et al. Neoproterozoic Subduction and Rifting on the Northern Margin of the Yangtze Plate, China: Implications for Rodinia Reconstruction. *Int. Geol. Rev.* **2004**, *46*, 817–832. [CrossRef]
48. Xiao, L.; Zhang, H.-F.; Ni, P.-Z.; Xiang, H.; Liu, X.-M. ICP-MS U-Pb zircon geo- chronology of early Neoproterozoic mafic-intermediate intrusions from NW margin of the Yangtze Block, South China: Implication for tectonic evolution. *Precambrian Res.* **2007**, *154*, 221–235. [CrossRef]
49. Yang, L.-Q.; Deng, J.; Qiu, K.-F.; Ji, X.-Z.; Santosh, M.; Song, K.-R.; Song, Y.-H.; Geng, J.-Z.; Zhang, C.; Hua, B. Magma mixing and crust-mantle interaction in the Triassic monzogranites of Bikou Terrane, central China: Constraints from petrology, geochemistry, and zircon U-Pb-Hf isotopic systematics. *J. Asian Earth Sci.* **2015**, *98*, 320–341. [CrossRef]
50. He, D.-Y.; Qiu, K.-F.; Santosh, M.; Yu, H.-C.; Long, Z.-Y.; Wang, J.-Y. Inhomogeneous crust-mantle interaction and Triassic tectonic escape of a Proterozoic microplate: A tale of the Bikou Terrane. *Lithosphere Int. J. Mineral. Petrol. Geochem.* **2021**, *396–397*, 106227. [CrossRef]
51. Whalen, J.B.; Hildebrand, R.S. Trace element discrimination of arc, slab failure, and a-type granitic rocks. *Lithosphere* **2019**, *348–349*, 105179.

52. Pearce, J.A.; Harris, N.B.W.; Tindle, A.G. Trace Element Discrimination Diagrams for the Tectonic Interpretation of Granitic Rock. *J. Petrol.* **1984**, *25*, 956–983. [CrossRef]
53. Zou, F.-H.; Wu, C.-L.; Gao, D.; Deng, L.-H.; Gao, Y.-H. Triassic granites in the West Qinling Orogen, China: Implications for the Early Mesozoic tectonic evolution of the Paleo-Tethys ocean. *Int. Geol. Rev.* **2022**, *65*, 1–33. [CrossRef]
54. Wang, Q.-F.; Deng, J.; Zhao, H.-S.; Yang, L.; Ma, Q.-Y.; Li, H.-J. Review on Orogenic Gold Deposits. *Earth Sci.* **2019**, *44*, 2155–2186, (In Chinese with English abstract).
55. Li, N.; Yang, L.-Q.; Groves, D.I.; Li, H.-X.; Yin, C. Tectonic and district to deposit-scale structural controls on the Ge'erke orogenic gold deposit within the Dashui-Zhongqu district, West Qinling belt, China. *Ore Geol. Rev.* **2020**, *120*, 103436. [CrossRef]